Technische Universität München

Lehrstuhl Energie Systeme

Diplomarbeit

Jonas Krüger
Matrikelnummer: 2821423

Definition of a system to extract hot gas from an entrained flow gasifier

Betreuer:	Dipl.-Ing. Mario Nakonz
	Philipp Kurowski M. Sc.
	Prof. Dr.-Ing. Hartmut Spliethoff
Ausgegeben:	17. Juni 2012
Abgegeben:	15. Januar 2013

Eidesstattliche Erklärung

Hiermit versichere ich, die vorliegende Arbeit selbständig und ohne Hilfe Dritter angefertigt zu haben. Gedanken und Zitate, die ich aus fremden Quellen direkt oder indirekt übernommen habe, sind als solche kenntlich gemacht. Diese Arbeit hat in gleicher oder ähnlicher Form noch keiner Prüfungsbehörde vorgelegen und wurde bisher nicht veröffentlicht.

Ich erkläre mich damit einverstanden, dass die Arbeit durch den Lehrstuhl für Energiesysteme der Öffentlichkeit zugänglich gemacht werden kann.

_____, _____ _____

Danksagung

An dieser Stelle möchte ich mich bei meinen Betreuern Mario Nakonz und Philipp Kurowski bedanken, die mir während dieser Diplomarbeit mit Rat und Tat beseite standen. Darüberhinaus bedanke ich mich bei dem Personal der Werkstatt und des E-Labors des Lehrstuhls für Energiesysteme. Zu guter Letzt gilt mein Dank meiner Familie und meinen Freunden, speziell Anna, Armin, Fee, Martin und Tom, die mich während dieser turbulenten Zeit unterstützt haben.

Abstract

This project work covers the design and construction of a new probe system for hot gas analysis in an entrained flow gasifier. The aim is a probe that can be used more flexibly than the present system. As a further aim, the condensation of trace materials has to be prevented. First, a short overview over current techniques to analyse the product gas in a gasification process is given. Continuing, the report describes the finding and assessing of several possible principles of hot gas extraction from a gasification process using simulations in ANSYS Fluent. The best performing design based on defined trace component condensation is built for a verification experiment and tested under controlled conditions in a tube furnace. Verification experiments comprise temperature measurements and analysis of retrieved samples via x-ray induced fluorescence. Temperature measurements show that the planned effect of mixture cooling is exceeded by far by convective cooling of the probe. Although simulations were promising, the approach is not applicable under current operating conditions due to problems with the measurement system. Furthermore, the amount of condensed trace material in the retrieved samples proves not to be sufficient for quantitative analysis via x-ray fluorescence. An alternative system to retrieve hot gas while maintaining it at high temperatures out of the gasifier is then modeled.

Zusammenfassung

Diese Diplomarbeit behandelt das Auslegen und Konstruieren einer neuartigen Probenahmelanze für die Heißgasanalyse von einem Flugstromvergaser. Das neue System soll flexibler einsetzbar sein als das aktuelle und das Auskondensieren von Spurenstoffen in der Lanze verhindern. Als erstes wird kurz der momentane Stand der Messtechnik in diesem Bereich vorgestellt, bevor verschiedene neue Probenahmelanzen vorgestellt und mit Hilfe von Simulationen in Fluent auf Eignung untersucht werden. Das System welches als am geeignetsten erscheint, in diesem Fall eines das auf defininiertem Auskondensieren basiert, wird mit Hilfe eines Rohrofenversuchs unter kontrollierten Bedingungen verifiziert. Die Verifikationsexperimente umfassen Temperaturmessungen und die Analyse von Proben mit Hilfe von Röntgenfluoreszenz. Die Temperaturmessungen zeigen dass die konvektive Kühlung der Probenahmelanze die eigentlich als Haupteffekt eingeplante Mischungskühlung bei weitem übertrifft. Aufgrund mehrerer Probleme mit dem System und der angewendeten Methode zum Analysieren von gewonnen Proben ist das Messsystem nicht zur Spurenstoffmessung während der Kohlevergasung geeignet, obwohl die Simulationen dies nahelegten. Darüberhinaus ist die Menge an kondensierten Spurenstoffen nicht ausreichend, um quantitative Aussagen mit Hilfe der Röntgenfluoreszenzanalyse zu treffen. Daher wird ein weiteres System zum Absaugen von Heißgas simuliert, welches das Gas unter Beibehaltung von hoher Temperatur aus dem Reaktor liefert.

Contents

List of Figures

List of Tables

Nomenclature

Latin letters

c_p	$^{kJ}/_{kgK}$	Specific heat
d	m	Diameter
h	$^{J}/_{kg}$	Enthalpy
n	-	Species concentration
p	$^{N}/_{m^2}$	Pressure
t	s	Time
u	$^{m}/_{s}$	Velocity
A	m^2	Area
C	m	Wetted Perimeter
D	$^{m^2}/_{s}$	Diffusivity
F	-	View Factor
L	m	Length
Q	J	Heat
T	K	Temperature
V	m^3	Volume
X	$^{kmol}/_{kmol}$	Molar fraction
Y	$^{kg}/_{kg}$	Mass fraction

Greek letters

α	$^{1}/_{m}$	Absorbtion coefficent
μ	$^{kg}/_{ms}$	Dynamic viscosity
ν	$^{m^2}/_{s}$	Kinematic viscosity
ρ	$^{kg}/_{m^3}$	Density
τ	s	Ring down time
σ	$^{W}/_{m^2K^4}$	Stefan-Boltzmann constant

Key figures

Re	-	Reynolds number
Tr	-	Transmittance

Indeces

vol	-	volumetric
re	-	reaction
sa	-	sample
ex	-	exhaust
gas	-	gasifier
fl	-	flush
hy	-	hydraulic
in	-	inlet
out	-	outlet
w	-	weight

Abbreviations

AAS Atomic Absorbtion Spectroscopy

AES Atomic Emission Spectroscopy

AMS Aerosol Mass Spectrometry

LES Lehrstuhl für Energiesysteme

RFA RöntgenFloureszenzAnalyse

LIF Laser Induced Florouscence

UDF User Defined Function

CFD Computational Fluid Dynamics

CAD Computer Aided Design

IGCC Integrated Gasification Combined Cycle

HoTVeGas Hochtemperaturvergasung und Gasreinigung

PiTER Pressurized high Temperature Entrained Flow Reactor

BabiTER Baby High Temperature Entrained Flow Reactor

TUM Technische Universität München

MFC Mass flow controller

EDX Energy Dispersive Spectroscopy

ppm parts per million

ppt parts per trillion

Mtoe Million tons oil equivalent

Btu British thermal units

GDP Gross Domestic Product

UDMI User Defined Memory

Chapter 1

Introduction

Confronted with rising global income and energy consumption, one needs to minimize the environmental impact of power plants to meet rising demand in a way that does not harm the planet for following generations (British Petroleum, 2006) (International Monetary Fund, 2012). Figures 1.1a and 1.1b show the close correlation between income and energy consumption levels. The required energy input to produce a given amount of value, the energy intensity, has fallen from 10.3 to 8.9 British thermal units (Btu) per $ of Gross Domestic Product (GDP) in the time between 1994 and 2006 (Energy Information Association, 2009). This is not enough to offset the rapid creation of wealth, especially in the developing world.

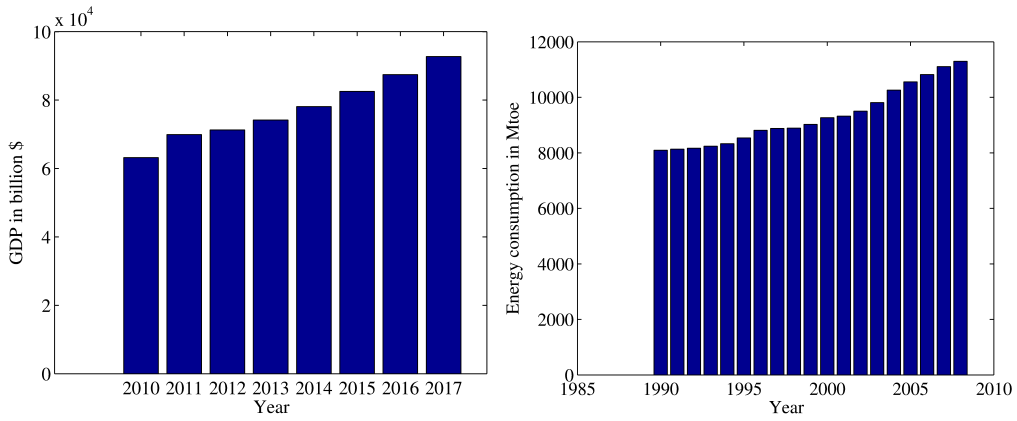

(a) **(b)**

Figure 1.1: Development of (a) Gross world product in bn $ and (b) Worldwide energy consumption in Mtoe

While renewable energy sources such as photovoltaics or wind power will play a big part in the future, high capacities of conventional power generation are still needed to counterbalance their uneven timely distribution and unpredictability. A process that is seen to have the potential to fulfill part of this role is the Integrated Gasification Combined Cycle

(IGCC). Coal is gasified in a gasification process and the product gas is used to fuel a gas turbine, whose waste heat is used to power a steam cycle. This process is called a combined cycle. The IGCC can generate electricity from coal reliably, economically and cleaner than conventional fossil fueled power generation processes Spliethoff (2010). Moreover, coal as primary fuel is widely available and evenly distributed throughout the world, decreasing the economic volitality of this resource.

In order to make the IGCC a viable alternative to the conventional coal fired power plants, several problems concerning the gasification have to be solved. The problem addressed in this work is the cleaning of trace components like alkali metals and chloride from the product gas. They are introduced via the coal, as these organic compounds contain a host of other elements besides hydrogen and carbon. These trace components lead to high temperature corrosion in the gas turbine and fouling in machine components upstream. The current process of gas cleaning is to cool the product gas to temperatures where the alkali metals condense and reheat the gas again. Because this decreases the overall efficiency of the process, it is desirable to clean the gas at or near gasification temperatures. To investigate the release behavior of trace components during gasification of coal is the goal of the Hochtemperaturvergasung und Gasreinigung (HoTVeGas) project of the Lehrstuhl für Energiesysteme.

The Lehrstuhl für Energiesysteme of the Technische Universität München (TUM) has two pilot-scale entrained flow gasifiers to conduct coal gasification under adjustable industrial conditions. In these gasifier the behavior of the synthesis gas and the influence of hot gas cleaning and CO_2 scrubbing (Spliethoff et al., 2011) can be analyzed. Results from these experiments will help to lessen the environmental impact of coal gasification and stress in the gas turbine. In addition, numerical and analytical models of the processes involved can be verified and adapted to fit the experiments, which can ease planning and optimizing such power plants.

1.1 Motivation

The predominant measurement systems for trace component analysis in industry and science use mass spectroscopy and x-ray induced florouscence analysis (Monkhouse, 2011). These systems are non-intrusive, have low detection limits and are capable of on-line measurements and therefore perfect for process control in industrial applications. However, they need optical ports or sampling flows. Under Pressurized high Temperature Entrained Flow Reactor (PiTER) and Baby High Temperature Entrained Flow Reactor (BabiTER) operation parameters of 1800 °C and 50 bar pressure, these requirements are hard to fulfill. But the measurement of gas components in different stages of the gasification process is indispensable for investigating the release of alkali compounds or effectiveness of different

cleaning techniques. Therefore, the gasifier of the Lehrstuhl für Energiesysteme has a port in the lower end through which a product gas retrieval probe can be inserted directly to take gas samples from different positions.

For the highest possible gasification temperatures of 1800 °C, the existing sample retrieval probe can only be used in the latest stage of the reaction zone due to the needed cooling power exceeding the heating power of the gasifier. Further, there is no way how the measured results correspond to the conditions at the sampling position, as the trace elements of interest condense in the probe system. Thus, a precise mapping of trace component concentrations to different parts of the reaction zone is difficult. A probe system that can take samples at every position under any mode of operation and conserves the condition of the trace components in the gas at the position the sample is taken would contribute to the understanding of gasification processes. To design such a system is the main aim of this thesis.

1.2 Outline

The reader is given a short introduction into the subject and the aim of this thesis in chapter 1. Chapter 2 covers the basics of gasification, followed by a brief overview over current gas extraction and trace component measurement methods in the field of gasification. The CFD-part begins with a description of the domain in chapter 3, continued by the settings and models used in ANSYS Fluent to simulate the different principles. A short analysis of mesh influence and turbulence modeling are also given. The User Defined Function (UDF) used to model condensation in porous media is presented in this chapter as well. Following, there are the results of the simulations and the conclusion which principle to build for verification with a tube furnace. A design of the verification system is given at the end of this chapter. The construction and description of the verification system, as well as the results of temperature measurements and condensation tests are described in chapter 4. All modifications made to the verification system are also presented. The results of the elemental analysis of the samples obtained conclude this chapter. Chapter 6 discusses the results and gives recommendations on how to build a hot gas extraction system for the BabiTER. The last chapter is the Appendix which contains the construction sketches, part orders, temperature distributions of the simulations as well as elemental analysis results.

Chapter 2

Gasification

2.1 Gasification processes

Gasification is the transformation of solid or liquid fossil fuels into gaseous form. Gaseous fuel has the advantage of being easier to distribute and usable in Combined Cycle power plants. The product gas is also used as a raw material for the chemical industry (Higman and van der Burgt, 2003). Gasification is achieved by partial oxidation of the coal feedstock under high temperatures, with the gasifying agent consisting of water, air, steam or any mixture of the three, depending on the process. The energy needed for the endothermic reaction can be supplied externally, called allotherm, or by supplying surplus gasifying agent and combusting part of the feedstock, called autotherm. Gasification can be divided into following sup-processes:

- Heating: The coal has to be heated up to temperatures at which all the subsequent processes happen.
- Devolatilizaition: Devolatilization is the process of removing all volatile components of the coal. It happens at temperatures ranging from 350 to 800 °C (Higman and van der Burgt, 2003). Depending on the rate of the heating up, it happens simultaneously with gasification or before it.
- Pyrolysis: The cracking of volatile components to smaller molecules.
- Gasification: Gasification is the process in which the remaining solid char in the coal particle is transfered into the gaseous state.

The ratio of energy still contained within the product gas to the energy content of the primary fuel ranges from 75% up to 88%, depending on the means to provide heat to the overall endothermic reaction and the desired product. Three main gasification processes dominate today: moving bed, fluid bed and entrained flow gasification. The processes differ in their suitable feedstock, diameter of coal particles, operation temperature and gasifying

agent. For further information, Higman and van der Burgt (2003) where the following short description of gasification processes is taken from, is recommended.

- Moving bed gasifiers were the first gasification processes to be employed in industrial processes. In moving bed gasifiers, coal particles of diameters ranging from 5 to 60 mm (Higman and van der Burgt, 2003) are dried, devolatilized and gasified at temperatures from 1100 °C to 500 °C in a counter-current. Steam and oxygen are used as gasifying agents. The process has a high cold gas efficiency but has moving parts, e.g. a stirrer to evenly distribute the coal, in the reactor increasing maintenance efforts. Coal conversion rates of 99 % can be reached. Whenever a product gas of high heating or high methane fraction of 10-15 % value is needed, this process is preferred. It is also used when the product gas is a raw material for subsequent chemical applications like the Fischer-Tropsch process.

- Fluid bed gasifiers use coal of a medium diameter of 6 to 10 mm as feedstock. The whole gasification process happens in the fluidized bed consisting of ash, coal and the gasifying agent which also acts as fluidizer. To migitate the problem of ash agglomeration, the operating temperatures are below the softening point of ash, 950 to 1100 °C. To compensate for the low temperatures, low rank coal is applied. An advantage of the fluid bed gasifiers is the possibility of desulphuring the gas in the reactor by adding lime to the fluid bed. Due to the high range of residence times, a small part of unreacted coal is removed with the ash, reducing conversion rates to 97 %.

- Entrained flow gasifiers operate under the highest temperatures of up to 1800 °C and have the highest conversion rates of higher than 99 % and the purest product gas. The residence time of the particles is the shortest of all three processes. They need very fine-milled coal particles of diameters smaller than 100 μm and have a high oxygen demand. Due to the high temperatures, the ash is present as slag and can be removed at the bottom of the reactor.

The preferred process for IGCC processes is the entrained flow gasification because of his high conversion rates and pure product gas. The relatively low heating value is of minor importance as the gas is used on-site.

2.2 Entrained flow gasification

For entrained flow gasification, the coal needs extensive drying and milling to small diameters before it can be used as feedstock. The main gasification reaction for real fuels after in an entrained flow gasifier after (Higman and van der Burgt, 2003) can be written as:

$$C_nH_m + n/2O_2 = nCO + m/2H_2 \tag{2.1}$$

where, for coal, $^{m}/_{n} \approx 1$ and therefore:

$$2CH + O_2 = 2CO + H_2 \tag{2.2}$$

Feedstock and gasifying agent are fed into the reactor in a concurrent flow. The high temperature and small diameter of the coal particles ensure high reaction rates. As the fuel has to enter the gas turbine combustion chamber at the same pressure as the air leaving the compressor, the product gas has to be pressurized. When using product gas to fuel a gas turbine, the process is run under pressure above the pressure in the gas turbine combustor, allowing for pressure loss in the gasifier and subsequent systems (Higman and van der Burgt, 2003).

2.3 Trace components in the product gas

The product gas of the gasification process contains a range of trace elements beside the main components CO and H_2, dependent on the feedstock composition, amongst other potassium and sodium as well as chlorine. The trace components are usually in the ash fraction of the feedstock and stem from the organic origin or sedimentary input during carbonization and are present in different compounds. Potassium and sodium chlorides are contained within the feedstock in varying magnitudes of concentration, the highest content being 5% of the ash fraction (Voss, 2008). While a big part of the mineralic material stays in the ash, some of these compounds go into the gas phase during gasification and are responsible for high temperature corrosion of the turbine blades (Spliethoff, 2010). While the alkali content of some product gases can reach up to 10-100 parts per million $(\text{ppm})_{vol}$ (Steffin, 1998, P.24), the upper allowed values for alkali content range from 0.5 ppm_{vol} down to 0.1 ppm_{vol} depending on the gas turbine manufacturer (Hauk, 2011). This gives the need to clean the product gas and measure the alkali content constantly. Cleaning of the product gas in present plants happens via:

- Washing: Leading the product gas trough a wet scrubber that subtracts soluble trace elements out of the flow
- Adsorption: Condensing the alkali at the surface of a particle and removing the particle via filtration
- Absorption: Adding sorbents to the product gas that absorb the alkali. The depleted sorbent is then filtered away at the hot gas filter

According to (Stemmler, 2010), all work at a temperature below 1000 °C or cool down the product gas, decreasing the thermal efficiency of the overall process. To overcome this limitation, there is a lot of research to develop an effective hot gas cleaning.

2.4 Hot gas extraction techniques

The extraction of unaltered hot gas for trace element analysis is a challenge. For lab-scale experiments as in (Bläsing and Müller, 2010) or (Müller, 2009), the sampling mechanism is constructed directly at the outlet of the tube furnace. All walls from the reaction zone to the sampling inlet having a temperature over the condensation temperature of the species to be analysed. This prevented the species in question from condensing out of the product flow. The methods described in Monkhouse (2011) that require a sampling flow are usually sampled isokinetically through a bent pipe made of ceramic or high temperature resistant steel inserted into the flow from the side as shown in figure 2.1.

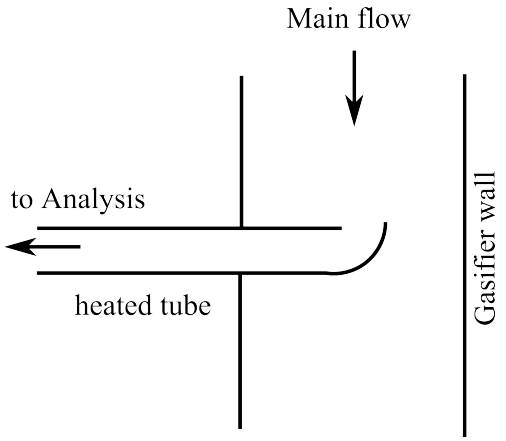

Figure 2.1: Isokinetic sampling with heated tube

Monkhouse (2011) mentiones a system in use for large gasifiers in which a small fraction of the product gas is diverted to a bypass, where a sampling mass flow can be obtained. Another system is the cooled probe as it is in use right now. This is primarily used for particle sampling and the condensation of trace elements in the probe is not prevented. Geisberger (2010) cites two systems that are used to sample particles and product gas. The first is an approach that mixes the product gas with a dilution flow that is pumped through a cooled pipe as it is shown in figure reffig:dilution. The second approach further improves this principle further by heating the tube with the sampling gas as soon as it gets out of the gasifier wall, preventing condensation of trace components before analysis.

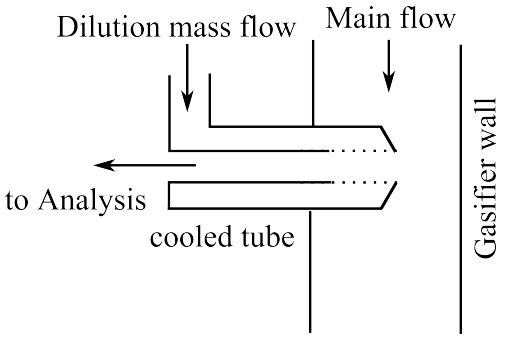

Figure 2.2: Sample probe principle after Mikkanen, taken from Geisberger (2010)

These extraction system still need one port for one axial position in the gasifier while allowing radial change of the sampling position. The system needed is one that allows for samples at different axial positions to be taken. Furthermore, none of the systems above can ensure that no trace components condense in the sampling probe.

2.5 Current measurement techniques

Current measurement techniques for trace components in the product gas of industrial processes rely on mass spectrographic analysis, absorption and x-ray or laser induced fluorescence measurements. The main advantages of these systems is their ability to measure on-line, having a high sensitivity and good temporal resolution. This makes them especially suited for process control applications and monitoring of cleaning techniques. Each system is suited for different types of species and environments. A review of measurement methods is found in (Monkhouse, 2011). However, the need for optical access or sampling flows decreases their applicability in the field of science. If the whole process of gasification is to be investigated, analyzation of the gas flow has to occur at different positions in the gasifier. The required number of optical or sampling ports is difficult and expensive to install in the gasifier, especially when high temperatures and pressures are involved. Therefore, a system that is able to take samples from different positions in the flow by repositioning the sampling intake is required.

2.5.1 Mass spectrometry

Aerosol Mass Spectrometry (AMS) relies on the different molar masses of atoms and molecules to differentiate between them. The basic principle is to break the sampled gas flow down into a single atoms to stop reactions between the individual compounds. Then, the compounds are ionized, formed into a molecular beam and led into a high vacuum environment. There, they are exposed to a magnetic field where they are diverted from their

original path via a quadrupole (Agilent Technologies, 2005) depending on their charge to mass ratio. The ionization occurs in a way that only one electron is removed from every sample gas compound. That way, each compound has an unique charge to mass ratio and therefore an unique deflection which can be detected via electron multipliers. Figure 2.3 shows a sketch of the principle.

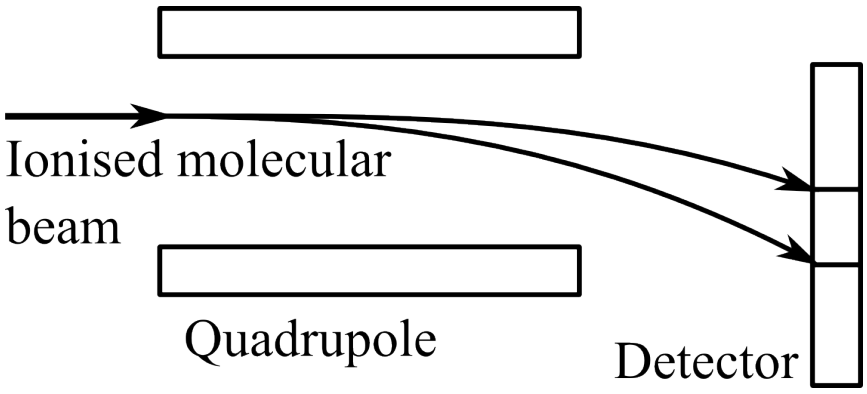

Figure 2.3: Principle of molecular beam mass spectrometry

There are many ways in which the sample mass flow is broken into single atoms and the ionization occurs. A good overview over the different variants of mass spectrometry can be found in (Monkhouse, 2011). Mass spectrometry features a low detection limit, good time resolution and applicability on high temperatures and pressures. The main disadvantage is its need for a sampling gas flow. One has to ensure that the gas condition does not change while sampling, for example by ensuring that the sampling gas does not interact with the sampling piping.

2.5.2 Absorption spectroscopy

Atomic Absorbtion Spectroscopy (AAS) uses the characteristic of atoms to absorb photons of only certain wavelengths. If the transmittance $Tr = I/I_0$ of the sample gas for light of a certain wavelengths is known the concentration of a species can be calculated using the Beer-Lambert law:

$$I = I_0 e^{-\alpha n l} \tag{2.3}$$

$$n = -\frac{\ln Tr}{\alpha l} \tag{2.4}$$

with I being the measured intensity, I_0 the incident intensity, α the absorption coefficient, n the molar concentration of the species to be measured and l the optical path length (Monkhouse, 2011). A sketch of the measurement technique can be found in figure 2.4.

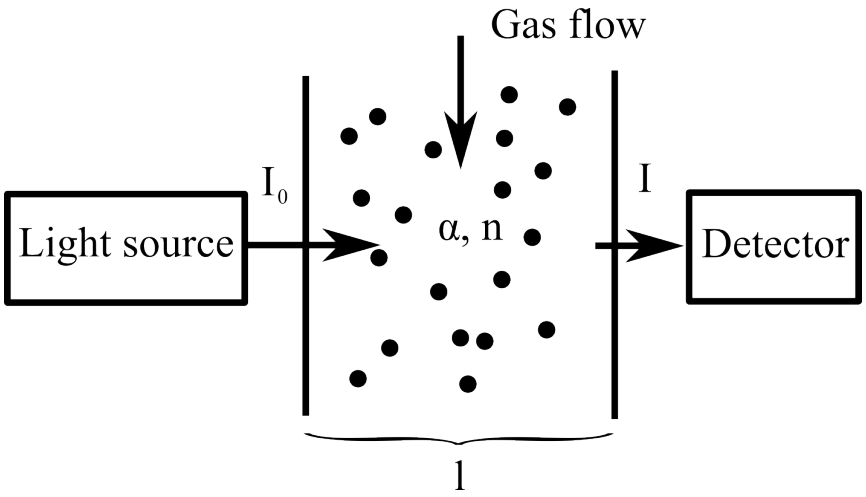

Figure 2.4: Principle of atomic absorption measurement

If the intensity change of a light signal is measured after passing through the sample gas with the absorption coefficient, the optical path length and incident intensity known, it is possible to calculate the concentration of the species directly. The light source has to emit light of the absorption wavelengths of the substance to be analyzed, so either a laser emitting several distinct wavelengths or a lamp emitting a wide spectrum is used. This approach has a detection limit of down to parts per trillion (ppt), but the absorption coefficient and the optical path length change with temperature and pressure. This requires extensive calibrations when the mode of operation is altered. Another approach using the absorption effect measures the ring down time τ until a photonic pulse that is reflected through the sample gas multiple times fades away. Absorption measurements always require multiple optical ports, increasing the costs for this approach.

2.5.3 Emission spectroscopy

Atomic Emission Spectroscopy (AES) uses the distinct energy levels of photons radiated when an excited atom undergoes the transition to its ground state. The excitation of atoms is carried out by lasers, giving the process the name Laser Induced Florouscence (LIF). The process can be used on-line and in-situ and some applications only require one port as the excited atom radiate their excess energy in every direction. However, for more sophisticated measurements several ports are required (Monkhouse, 2011). Figure 2.5 shows the principle of laser induced florouscence.

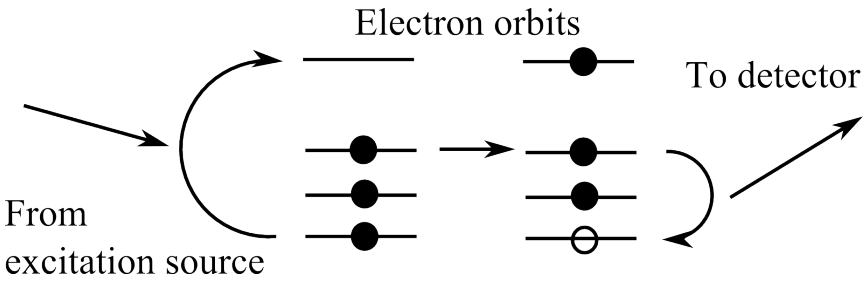

Figure 2.5: Principle of x-ray induced flouroscense

When an radiation hits an atom with a certain energy, an electron is removed from one of its inner shells. An electron from the outer shells jumps into the free orbit. The energy difference between the two orbits is then radiated away, which is detected by a photo multiplier. This kind emission spectroscopy is called Energy Dispersive Spectroscopy (EDX).

The other application of emission spectroscopy is off line measuring by pressing material into a pill and exciting atoms in a small area of the upper surface layer of the pill and measuring the florouscence. This is used to analyze the elemental composition of samples obtained by experiments as done in section 5.5.

Chapter 3

CFD work

To analyze the performance of different hot gas extraction systems, they are simulated using the commercial Computational Fluid Dynamics (CFD) software Fluent. Fluent gives the user a range of different approaches to model a flow with reactions, heat transfer, radiation, discrete phases and the possibility to augment the program with own models and functions (Ansys, 2012). It is integrated into the Ansys software and allows the user to do parameter studies that involve the changing of parameters, boundary conditions, mesh conditions and geometries. A simulation of a case that has a set of parameters is called a design point. Each design point can be investigated independently or numerical results of the simulations can be imported into Fluent allowing for comparison between design points.

3.1 Geometry and meshing

The geometry is constructed using the Ansys Design Modeler or imported from Computer Aided Design (CAD) software. Figure 3.1 shows the part of the PiTER that is modeled in the Design modeler. The whole reaction zone is modeled, as is the quench. To ensure a developed flow field, the gasifier wall is modeled longer than it is in reality. The atmospheric version of the gasifier, the BabiTER, has a similar geometry and gasification happens at ambient pressure. The process of dividing the geometry in finite volumes is carried out using the Ansys Mesher. Setting up boundary conditions, solution methods and solving the equations is done in Fluent.

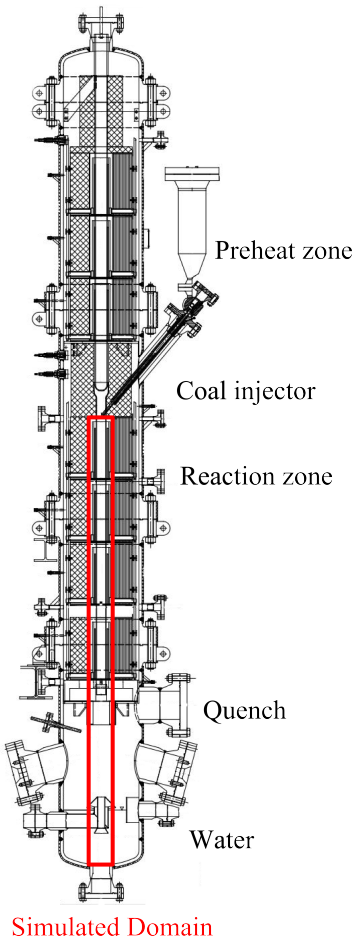

Figure 3.1: Red box: Domain simulated in Fluent, graphic from (Richter, 2008)

This physical geometry is transferred into the domain shown in figure 3.2. The probe is then replaced for each principle.

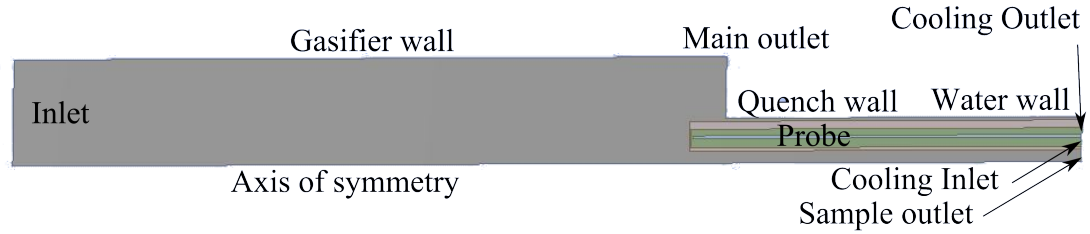

Figure 3.2: Geometric Model in Ansys Design Modeler

The flows into the domain via the Inlet on the left and leaves on the right through the sample and the main outlet. The boundary conditions for the part of the geometry that stays the same for all simulations is described in section 3.2.5. All different designs are first

simulated with the geometry from the PiTER. The best performing system depending on defined condensation is then modeled for the verification system in the tube furnace. This results primarily in a reduction in the preheating length in the geometry from 1 m to 0.4 m in the tube furnace. Furthermore, the reaction tube diameter for the PiTER is 70 mm while the tube furnace has a diameter of 93 mm.

3.2 Case set-up

In order to assess if any new design can fulfill the requirements, a series of simulations using Fluent are conducted. The probe system has to fulfill two contradicting goals: To lower the temperature of the probe mass flow to decrease the rate of the gasification reaction, and to keep the trace materials from condensing uncontrolled in the probe system. Furthermore, the required cooling power for the probe system has to be lower than the available heating power of the gasification reactor for every position of the probe and gasifier temperature.

3.2.1 General Settings

The whole process is regarded as steady state. As the parts of the tube furnace and the probe as well are axisymmetric, the problem is modeled using a two-dimensional, axisymmetric domain. Fluent allows to enable several models in order to best approximate the problem at hand. All models used in the simulation are mentioned in a short fashion. All other models or values not mentioned in the submenus are retained at their original values. Because heat transfer is the main process affecting the flow, the energy equation in the Fluent setup is activated. This enables the enthalpy calculations, heat dependence of certain material properties such as density and heat transfer via convection and conduction.

3.2.2 Species

In the species submenu, volumetric and surface reactions are activated. The thermodynamic data for the reacting species are taken from (NIST Webbook, 2012). However, as the reaction rate is calculated using UDFs, only values for density, heat capacity, thermal conductivity, diffusivity and molecular weight are of importance. Two reactions are defined, one is the volumetric phase change of the trace alkali component, the other the surface condensation. The volumetric reaction is the phase change of trace components in the flow from gaseous to liquid, and the surface reaction from gaseous to liquid on the getter surface. For both reactions, all reaction data is retained at their standard values as the reaction itself is calculated with the UDFs described in 3.4.1. Because the UDF use values for each species, the order how the species are defined is of great importance for the functioning of the UDF. Tabular 3.1 gives an overview in which order to define the species in the mixture

template submenu for the calculations of sodium and potassium chloride. The order has to be the same as in the table, with the bulk species having to be at the bottom of the fluid species.

Table 3.1: Defined materials order in material editor

NaCl-setup	KCl-setup
Fluid species:	
NaCl <g>	KCl <g>
NaCl <l>	KCl <l>
Air/Nitrogen	Air/Nitrogen
Solid species:	
NaCl <s>	KCl <s>

NaCl <g> is gaseous sodium chloride, NaCl <l> and NaCl <s> can have the same values as NaCl <g> as the UDF does not take into account any material data other than the molar weight. If the condensation of KCl has to be calculated, every variety of NaCl is to be replaced by KCl. Alterations required in the UDFs are explained in 3.4.1. The synchronous calculation of sodium and potassium chloride is not implemented.

3.2.3 Radiation Discrete Ordinates

Radiation heat transfer is the main heat transfer for high temperatures. The heat transfer of two bodies 1 and 2 via radiation is calculated via:

$$\dot{Q} = \sigma F_{1\to 2}(T_2^4 - T_1^4) \tag{3.1}$$

with σ being the Stefan-Boltzmann constant, F the view factor from body 1 to 2 and T the temperature of body 1 and 2 respectively. In the Discrete Ordinates model, the radiative heat transfer of each cell is calculated individually by dividing the field of view of every cell into discrete parts and calculate the heat transfer in this direction. The number of discrete parts and their resolution are chosen by the user. The values used for the simulations are found in appendix 3.2 and are used in all simulations conducted in this work.

3.2.4 Material properties

To compare the simulations to the calculated heat flows of the thesis by (Donaubauer, 2012), similar material properties as in the analytical approach have to be used. The material properties are shown in tabular 3.3. Some properties such as the emissivity are

Table 3.2: Values for radiation setup

Radiation	
10 Flow iterations per radiation iteration	
ϕ-divisions	4
ϕ-pixelation	2
θ-divisions	4
θ-pixelation	2

only available as a range of values. Where sources give a range of values for material properties, the values used are the ones most negatively affecting the performance of the system, e.g. the insulation is simulated with a heat transfer coefficient at the higher end of the range.

Table 3.3: Properties of the materials used in the simulations, the values for ceramic taken from makeitfrom.com (2013)

Property [Unit]	Air	Oil	Ceramic	Steel
ρ in $^{kg}/_{m^3}$	ideal gas	850	4000	7850
λ in $^{W}/_{mK}$	0.0242	0.102	30	20
c_p in $^{J}/_{kgK}$	1006	2400	800	500
ϵ	x	x	0.9	0.4

3.2.5 Boundary conditions

The boundary conditions are chosen so that the simulations depict the main properties of the flow in the gasifier with sufficient accuracy. The main walls that transfer heat to and from the flow are modeled as no-slip walls with a constant temperature. The gasifier wall has a temperature ranging from 1200 to 1800 °C. The quench wall temperature is set to the boiling temperature of water at 1bar pressure 100 °C. As the maximum temperature for the quench water is required to be under 80 °C in the gasifier specification, the temperature for this wall is set to this value. All inlets are set to mass flow inlets. All outlets are pressure outlets with the sample and exhaust flow outlet having a target mass flow rate to set the mixing ratio of flush and product gas at the probe tip. All interfaces between two solid zones or a solid and a fluid zone are modeled as coupled walls, enabling heat transfer. The interfaces between two fluid or a fluid and a porous zone are set to interior to enable mass transfer. Figure 3.3 shows an overview of the boundary conditions, all lines in the graphic that have no description to them are coupled walls.

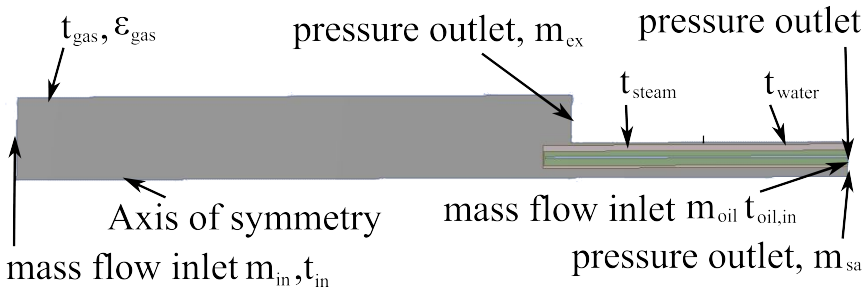

Figure 3.3: Boundary conditions of the case

The mass flow at the pressure outlets is a targeted mass flow, meaning Fluent is attempting to obtain the mass flow via gauge pressure variations.

3.2.6 Solution methods

The main flow equation is the semi-implicit scheme and all equations are discretized with the second order upwind scheme. Relaxation factors are all retained at their standard values or set to 0.8 if the standard values are higher. To monitor convergence, a surface monitor with the area averaged temperature in the oil outlet is created. Convergence criteria are disabled and the simulations stopped when the decrease in residuals flatten out and the area averaged temperature shows no transient behavior.

3.3 Pretests

Pretests are conducted to find the optimal setup for the simulations, modeling the case with sufficient accuracy. The properties evaluated are the mesh influence on the simulation, turbulence modeling and particle injection. The implementation of an UDF to model condensation in a porous medium is also tested.

3.3.1 Influence of mesh refinement

The way in which a geometry is meshed influences the computational time, convergence rate and quality of results. To ensure that the geometry is meshed with sufficient refinement and quality, a selected case of the current probe system is simulated with three meshes of increasing cell number, leaving the settings in Fluent unchanged. The heat transfer into the cooling system and the overall temperature distribution are then compared. An overview over the meshes is found in figure A.2

Table 3.4: Mesh attributes

Mesh	No. of Elements	Avg. orthonogality	Cooling power
Rough	88642	0.98	9.2 kW
Default	92799	0.85	9.74 kW
Fine	172971	0.86	10.2 kW

While the rough and default mesh converge within similar time ranges, the fine mesh needs significantly longer to converge. As the parameter studies for all principles and modes of operation amount to many cases to simulate, the default mesh is chosen for the preliminary studies and the fine mesh for the next stage of the development process.

3.3.2 Turbulence Modeling

To assess if turbulence modeling is required for the cases simulated, the Reynolds number of the flows involved is calculated with

$$Re = \frac{d_{hy} \cdot u}{\mu} \tag{3.2}$$

with the hydraulic diameter

$$d_{hy} = \frac{4A}{C} \tag{3.3}$$

with A being the cross section of the tube and C the wetted perimeter. Table 3.5 lists the values used for the Reynolds number calculations and the numbers itself. The values for the velocity and viscosity are taken from the calculations performed in (Donaubauer, 2012), with the air velocity taken from first simulations. The diameters are taken from the present geometry. The radiation modeling is set do Discrete Ordinates with the values found in 3.2. The gasifier wall temperature is set to 1200 °C and the main mass flow to 1 g/s with the sample mass flow accounting for 0.1 g/s and the main outlet mass flow to 0.9 g/s. The oil mass flow is 70 g/s.

Table 3.5: Expected Reynolds numbers for flows in the simulation

Flow	Velocity in $\frac{m}{s}$	Viscosity in $\frac{m^2}{s}$	Hydraulic diameter in m	Reynolds number
Air	1.4	$5 \cdot 10^{-5}$	0.07	≈ 560
Oil	1	$6.9 \cdot 10^{-7}$	0.002	≈ 3000

For the case at hand, the air flow is laminar and the oil flow is in the transition range $2300 < Re_{krit} < 10000$. Therefore, a short simulation to test the influence of turbulence

in the air zone is carried out. Figure 3.4 compares the flow lines for air for a laminar and turbulent calculation of the same flow, figure 3.5 the temperature distribution at the probe tip. The used turbulence model is the k-ϵ RNG model. RNG enhances the normal k-ϵ model by accounting for strained flows and swirls in the flow (Ansys, 2012), some of which are expected in the case at hand. Furthermore, the RNG model accounts better for viscosity in low Reynolds number environments as the flow problem present.

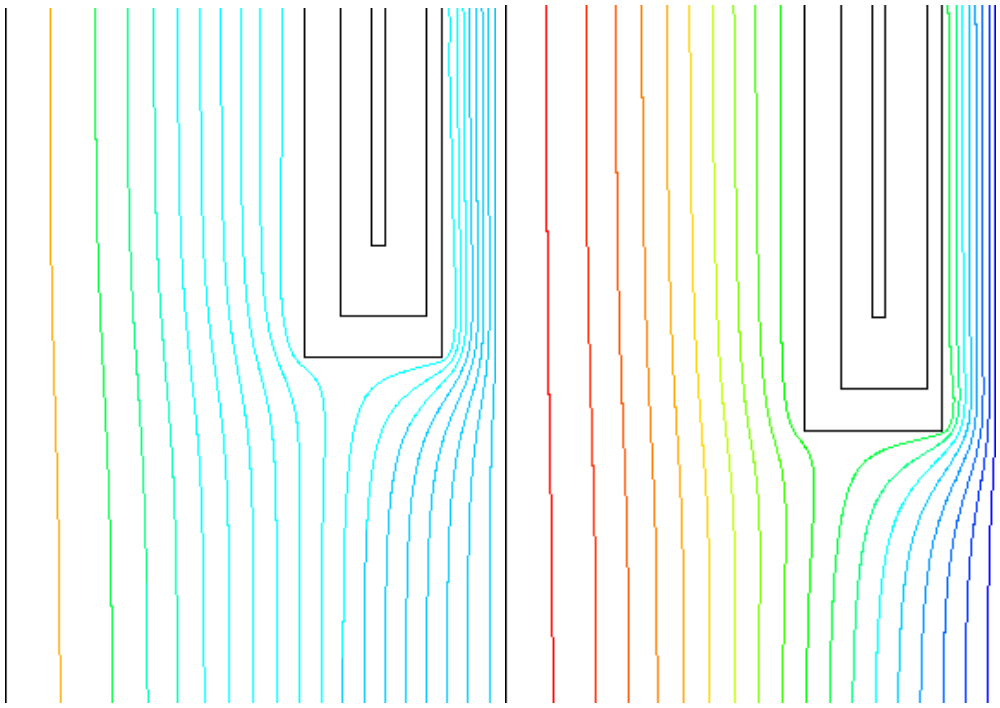

Figure 3.4: Comparison of path lines for the laminar and turbulent model: (a) Laminar model, (b) Turbulent model (k-ϵ, RNG)

The figures 3.4a and 3.4b show the pathlines of virtual, massless particles released at the main flow inlet. They are in good agreement for the two models.

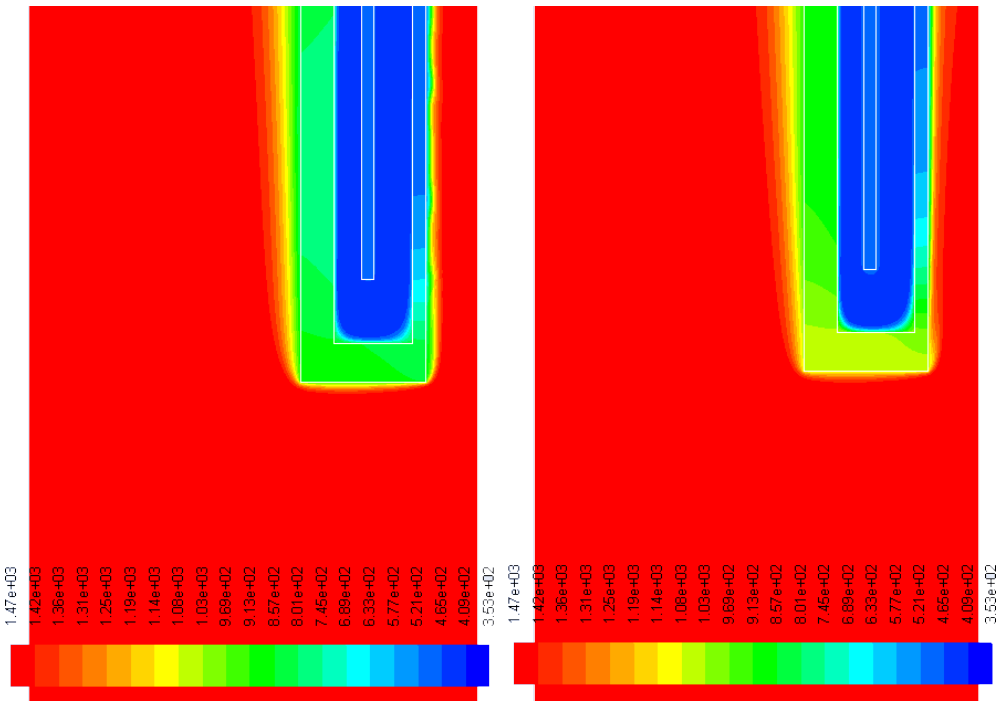

Figure 3.5: Comparison of temperature distribution for the laminar and turbulent model: (a) Laminar model, (b) Turbulent model (k-ϵ, RNG)

In figures 3.5a and 3.5b the temperature distribution at the probe tip is shown for the laminar and turbulent model is shown. The sample mass flow cools down slightly faster in the turbulent case. The heat transported out of the system with the laminar model is 9416 W while that of the turbulent model is 10577 W. As the flow in the probe is turbulent, the turbulent model is used in the simulations and the air zone is set to laminar in the zone settings.

3.3.3 Discrete Phase

Inert particles are injected into the flow to assess which particles can follow the flow into the sampling probe. As the ratio of alkali present in the ash can be up to 5%, ash particles on the surface of the sample would influence the elememental analysis heavily. The particles are injected via the main flow inlet and with the same velocity and temperature as the bulk gas. Brownian motion and drag law are enabled. Diameters are distributed with the rosin-rammler logarythmic function with the smallest diameter being 10^{-6} m, the maximum 10^{-4} m and the mean being 10^{-5} m. Figure 3.6 shows the particle distribution at the probe system inlet.

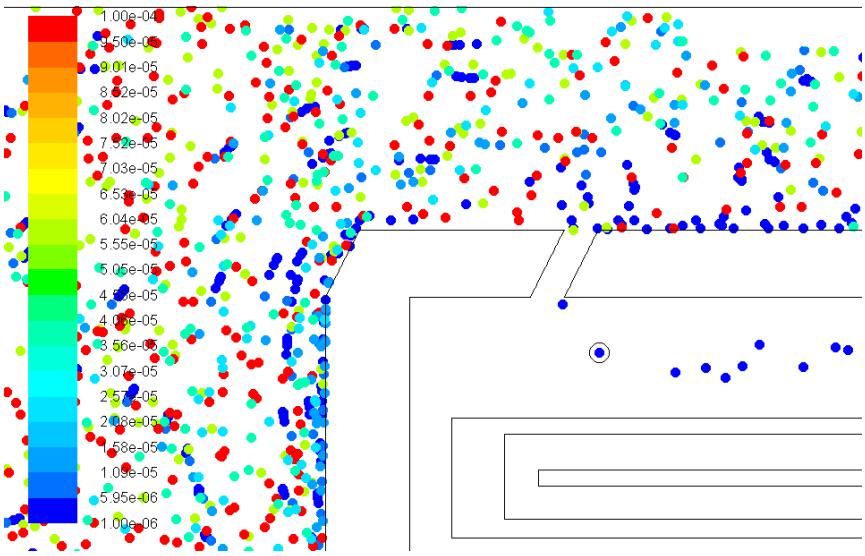

Figure 3.6: Particle tracks of different particle diameters at the probe tip at an average air flow velocity of 1m/s

Only the smallest particles can follow the air flow into the probe system if the flow is diverted sideways into the probe, although at the cost of losing the property of isokinetic sampling.

3.4 User defined function

Fluent uses the Arhennius ansatz to models chemical reactions. The physical reaction of condensation is not implemented in Fluent. A UDF for the condensation of trace elements using Antoines law of steam saturation and condensation of excess material exists, but can be only applied to volumetric condensation. The UDF was augmented by a second UDF which prescribes the calculated values into the reaction rates for surface reactions in the porous zone. The calculations are still the same as in the volumetric case, but the resulting material is no longer transported away but stays in the porous zone. The current program requires the user to define 3 User Defined Memory (UDMI) in Fluent.

3.4.1 Volumetric condensation

This UDF loops over every fluid of the cell and calculates the volumetric reaction rate according to Antoines ansatz of saturation pressure (Antoine, 1888). The saturation pressure of the gaseous trace alkalies in dependence of the temperature is modeled using following equation:

$$\log_{10}(p_{sat}) = A - \frac{B}{C+T} \tag{3.4}$$

with the parameters for A, B and C according to (NIST Webbook, 2012):

Table 3.6: Antoines coefficients for NaCl and KCl

Alkali	A	B	C
NaCl	3.56682	5200.904	-317.409
KCl	4.61668	6910.833	-176.083

yielding the trend for the saturation pressure for a total pressure of 1 bar shown in figure A.1. Therefore, sodium chloride condensates at higher temperatures as potassium chloride. Partial pressure in a gas is calculated with:

$$p_i = p_{tot,cell} X_i \Rightarrow X_{i,sat} = \frac{p_{i,sat}}{p_{tot,cell}} \tag{3.5}$$

thus, if the partial pressure of the component is higher than the saturation pressure of the component at this temperature, the excess component has to undergo a phase change. The assumption for this UDF is that there is enough activation energy and condensation seeds in the flow for condensation to occur. The reaction rate is then calculated as:

$$r_{reaction,i} = 0.01 \rho_{cell} D_i \frac{(X_{i,cell} - X_{i,sat,cell})}{d_{cell} Y_i} \tag{3.6}$$

This is the volumetric condensation of gaseous NaCl. ρ_{cell} is the local density, D_i the diffusivity, $X_{i,cell}$ the molar fraction of the component in the flow,$X_{i,sat,cell}$ the saturation molar fraction of the component, d_{cell} the cell diameter and Y_i the mass fraction of the component in the flow. The differentiation between liquid NaCl and solid NaCl as product is not made as only the rate of deposition and subtraction from the flow are of concern for this simulation. The reaction rate is stored in an user-defined memory for every cell. If the algorithm loops over the porous zone, the volumetric reaction rate is set to zero, as the reaction there has to be written by the surface reaction UDF. Moreover, calculated values as the saturation pressures for the species in question are stored in user defined memory for post processing. As the UDF does not loop over every reaction, to change the UDF from condensation of sodium chloride to potassium chloride one has to change the species in the mixture template to KCl as described in 3.2.2. In the DEFINE_VR_RATE, the upper section containing the calculations for sodium chloride have to be commented and the section for potassium uncommented. No changes have to be done in the DEFINE_SR_RATE UDF.

3.4.2 Condensation in porous media

This UDF loops over all surface or porous reactions. If a cell is in the porous zone, the present reaction rate is read from the user-defined memory saved in section 3.4.1. This way, the trace component is condensed in the porous zone and subtracted from the flow. Applied boundary conditions for this case are a wall temperature of 1400 °C , a main inlet mass flow of 1 g/s, a flush mass flow of 0.8 g/s, a sample mass flow of 1 g/s and a cooling mass flow of 30 g/s. This results in a exhaust mass flow of 0.8 g/s and a mixing ratio of 0.2. The species load for sodium chloride and potassium chloride is 2 ppm_w. The temperature distribution at the probe tip for this case is shown in figure 3.7.

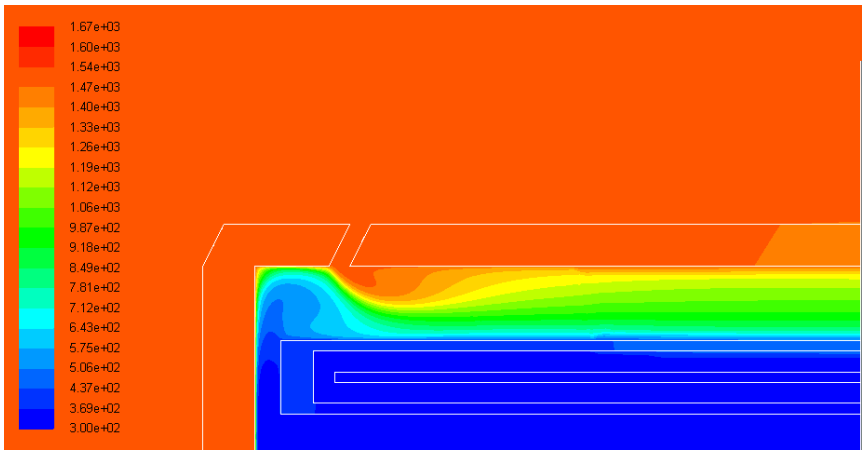

Figure 3.7: Temperature distribution at probe tip for the simulation of the tube furnace experiment (T_{wall}= 1400 °C, values in K)

The hot gas entering the probe system is rapidly quenched and the bulk of the sampling mass flow is cooler than 1073 K 2 cm downstream of the sample inlet. However, there is a high temperature gradient from the cool probe to the hot ceramic insulation. The UDF calculations of the condensation rates for sodium and potassium chloride are shown in figures 3.8a and 3.8b.

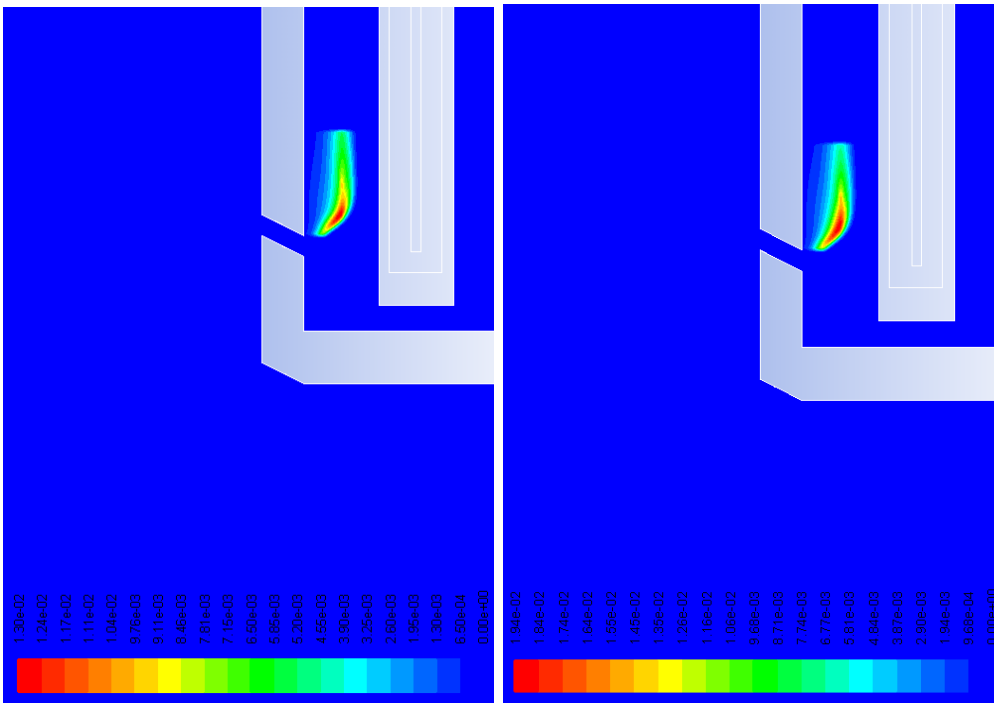

(a) **(b)**

Figure 3.8: Comparison of condensation processes of: (a) NaCl and (b) KCl

Resulting from the different values for the saturation pressure formula in 3.4, the corresponding condensation areas differ slightly. The highest rate of condensation is roughly found in the position where the product gas flow and the flush flow mix directly and the ratio of condensable species and temperature reduction is the best. The rate of condensation direct at the ceramic insulation is low due to the product mass flow shielding the area from the cold flush mass flow. As the product mass flow containing condensable species does not reach to the probe, no condensation can happen there. Because the condensation rate depends on several factors as the surface to volume fraction in the porous media or other factors influencing the condensation rate, no clear predication can be made for the species loading of the sampling mass flow. Figures 3.9a and 3.9b show the species loading for the simulation.

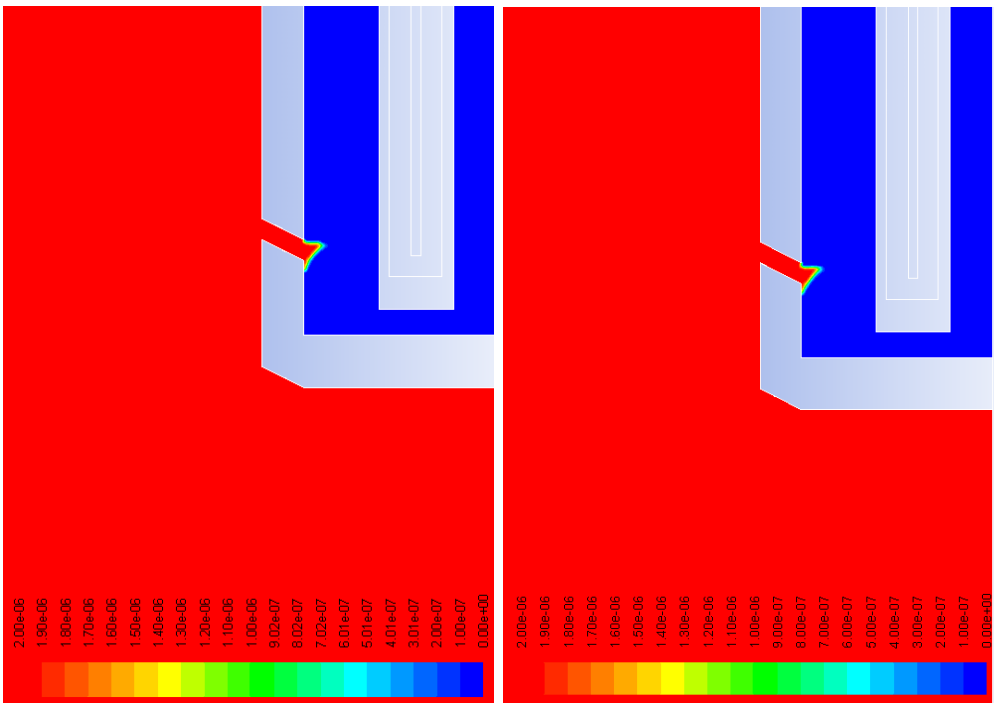

(a) **(b)**

Figure 3.9: Comparison of NaCl and KCl mass fractions in main flow (Red:2 ppm, blue: 0ppm)

Sodium and potassium chloride are rapidly subtracted from the main flow. Only the outer third of the getter surface is exposed to the alkali chlorides. The getter substracts all alkali chlorides from the sampling mass flow.

3.5 Principles simulated

Following principles to either transport the sample gas out of the gasifier retaining a constant temperature or condense the trace components in a distinct location are simulated:

- The current probe sample system used in figure 3.10a
- Acceleration of the sample gas flow to prevent phase change and reaction in figure 3.10b
- Insulation of the sample probe interior in figure 3.10c
- Insulation of the sample probe exterior and cooling with air in figure 3.10d
- Heating of the sample gas flow in figure 3.10e

- Defined condensation of sample gas trace components in a getter in figure 3.10f

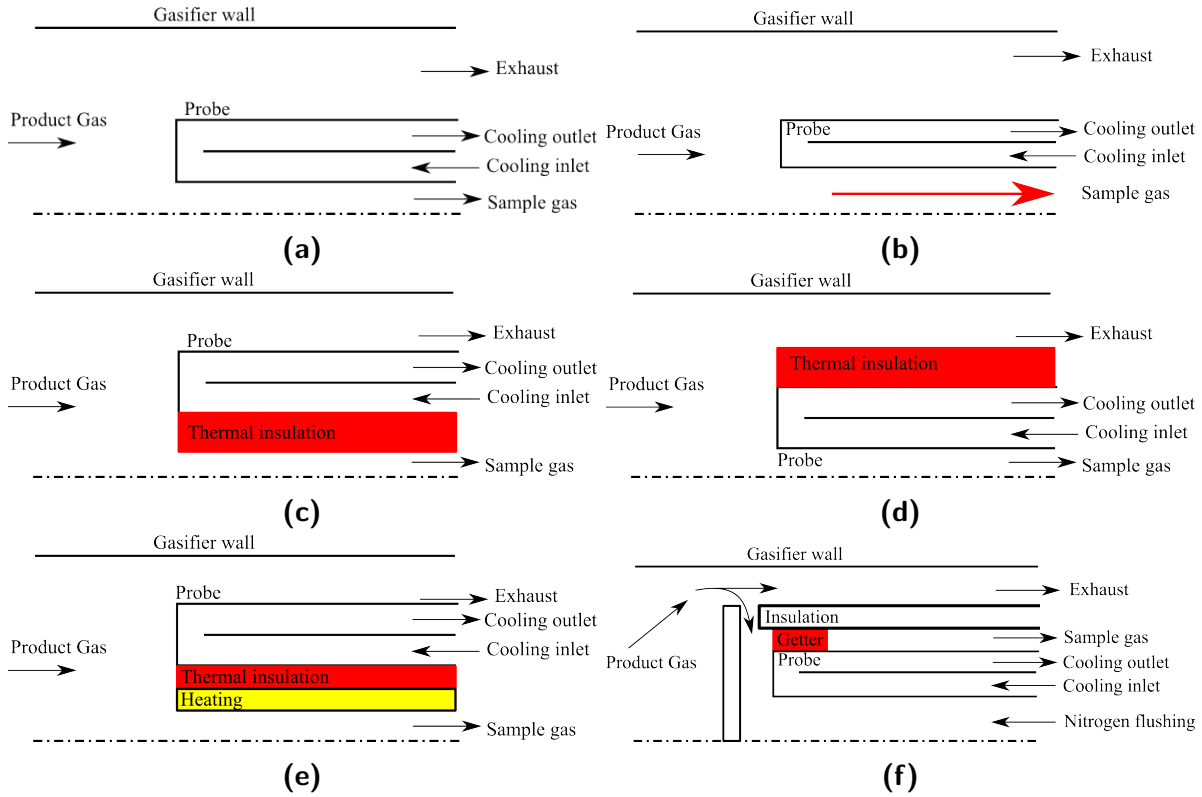

Figure 3.10: Principles to be simulated: (a) current system, (b) acceleration of sample mass flow, (c) insulation of probe inner, (d) insulation of probe outer, (e) sample mass flow heating (f) defined condensation

The main changes in design in comparison to the current system in figure 3.10 are displayed in red. Each principle was simulated in different sub designs such as insulation thickness, exposure length and gasifier temperature to assess each performance. The thermal distributions shown for each principle are for their best performing geometry at 1800 °C gasifier temperature and 100 and 1100 mm exposure length in the reaction zone.

3.5.1 Current sample retrieval system

The operation of the current sample retrieval system is modeled in Fluent using the same assumptions as in a project work that calculates the heat transfer into the probe using Excel. The geometry is taken from The results are in good accordance and show the inability of the current system to be applied above certain temperatures and only up to a certain length in the reaction zone. This stems from two restrictions: the cooling oil may

not be heated above 300°C to avoid evaporation and the cooling power should be below the maximum heating power of the gasifier. The maximum heating power in the reaction zone is 21 kW resulting from three graphite heaters with a power of 7 kW each. The cooling power is calculated by:

$$\dot{Q}_{cooling} = \dot{m}_{oil} h_{oil,out} - h_{oil,in} = \dot{m}_{oil} c_{p,oil} (T_{out} - T_{in}) \tag{3.7}$$

Which, in the case for a wall temperature of 1800°C and 1 m exposed length of the probe, amount to a needed cooling power of around 55 kW, making this design dysfunctional. Furthermore, the sample gas flow is quenched rapidly due to the small diameter of the sampling pipe, resulting in a high surface to volume ratio. This leads to condensation of trace components at the tip of the sample pipe. The thermal distribution at the probe tip for the current probe system at 1800 °C for 100 and 1100 mm exposure length is shown in figures 3.11a and 3.11b respectively.

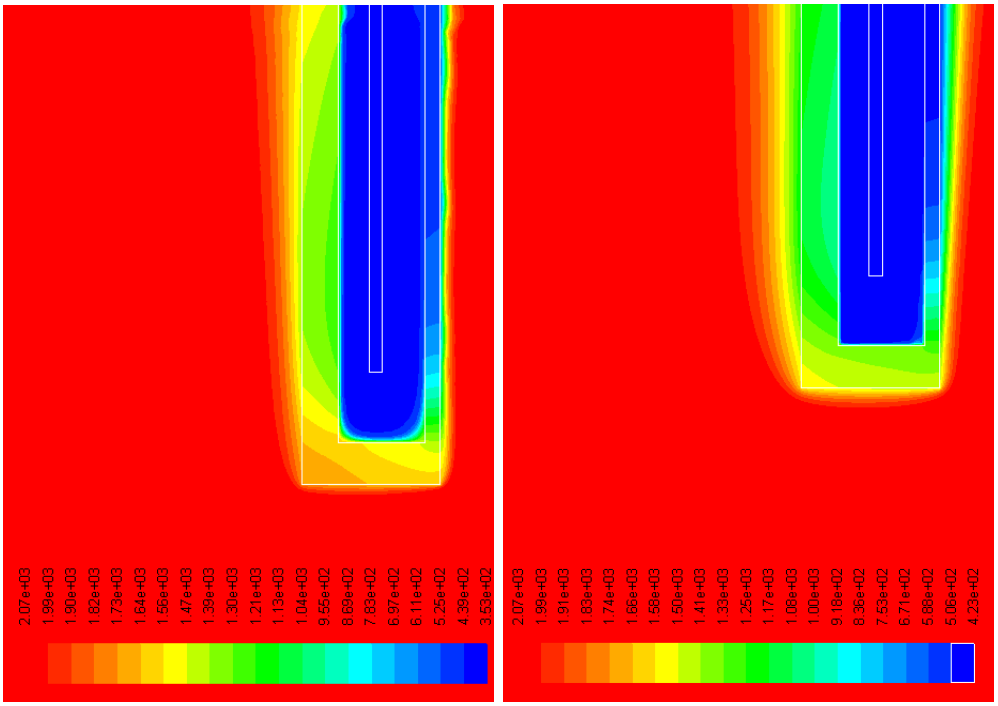

(a) **(b)**

Figure 3.11: Thermal distribution at probe tip for current system for (a) 100 mm and (b) 1100 mm exposure at 1800 °C

3.5.2 Comparison with analytical result

In a earlier work at the Lehrstuhl für Energiesysteme (LES) the cooling of the current probe system was designed and built using an analytical approach calculating the heat transfer to the probe within Excel (Donaubauer, 2012). This was done to obtain the boundaries of operation where the probe would not be damaged and the resulting cooling power would not exceed the heating power at hand. Several temperatures and probe positions (length with which the probe is exposed to the gasifier wall, rack length were calculated. The boundary conditions, material properties and basic values that were used in the calculations are transferred into Fluent and the heat transfer into the probe simulated. A comparison of the heat transported into the probe is found in figure 3.12. Gasifier temperatures are 1200, 1400, 1600 and 1800 °C, the flow velocity 1 $^{m}/_{s}$, gasifier wall emissivity 0.9 and the oil mass flow 7 $^{l}/_{min}$.

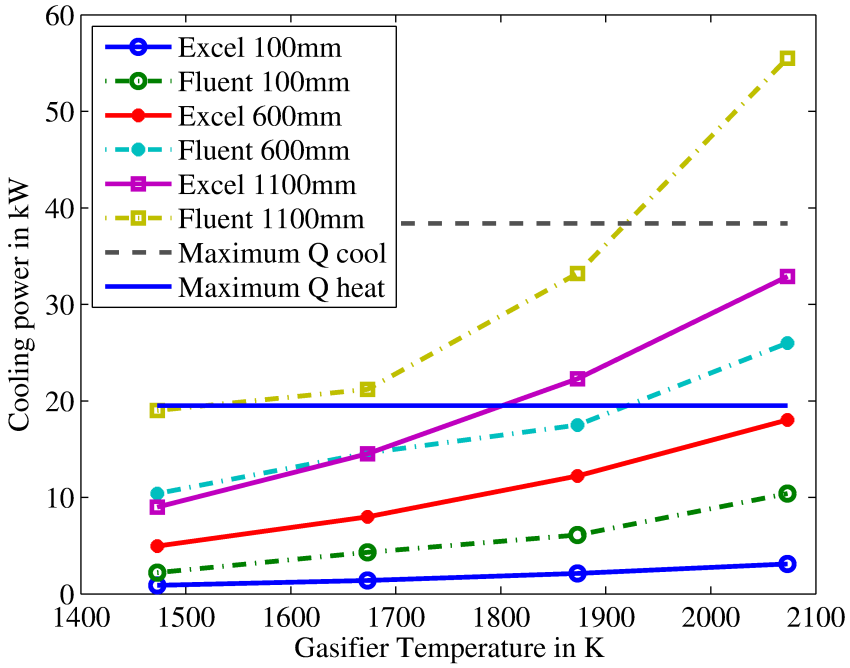

Figure 3.12: Comparison of cooling power over rack length at different temperatures. ($\dot{m}_{oil} = 7^{l}/_{min}$)

Though showing similar trends, the heat transfer simulated by Fluent is considerably higher than the Excel calculations. This severely limits the suitable conditions in which the probe system can be used. Several factors contribute to this outcome: while the Excel calculations set a constant mean flow velocity of 1 $^{m}/_{s}$, the velocity in Fluent changes dependent on the flow field although care was given to achieve similar velocities at the

outer hull of the probe. As Donaubauer (2012) mentions, the flow in the real gasifier is dust laden, so the real radiative heat transfer is lower than the simulated one.

3.5.3 Insulation of probe system interior

The main problem of this principle is the rapid quenching of the probe mass flow once it is in the inner pipe, as the probe mass flow is very small and the walls of the cooled probe are in acute vicinity. The flow cools from about 1700 K to the wall temperature of 600 K within the first half meter of the probe system. A better insulation between probe mass flow and probe wall has the potential to decrease the quench rate, so that the probe mass flow passes the probe system within the desired temperature range. Figure 3.13 shows the sketch of this principle.

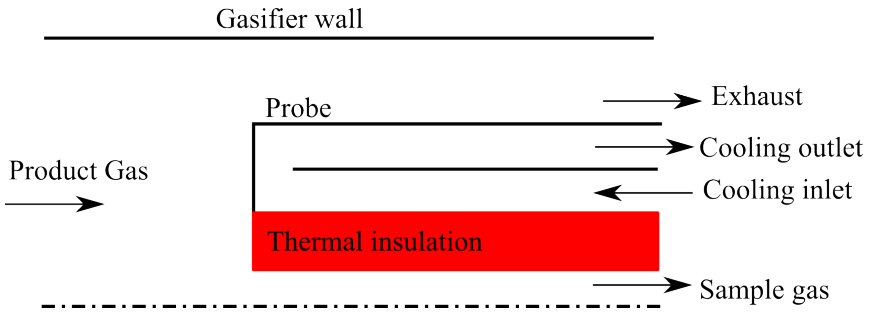

Figure 3.13: Principle of insulation of the inner gas flow

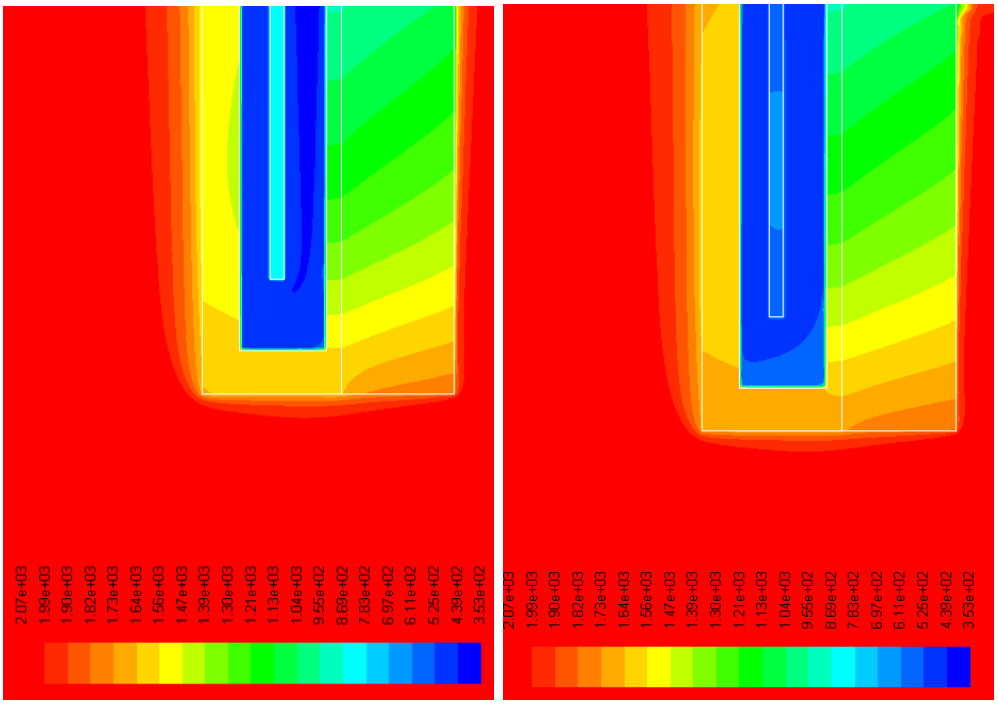

Figure 3.14: Thermal distribution for the insulated sample mass flow for (a) 100 mm and (b) 1100 mm exposure at 1800 °C

Simulations of this principle shows that the required isolation breaks the geometric constrains given by the gasifier tube diameter of 70 mm. The efficiency of insulation is reduced because thicker insulation reduces the gab between probe and gasifier wall, increasing the radiative heat transfer. While the temperature of the insulation quickly approaches the temperature of the cooling oil, the outer wall of the probe is still exposed to the same temperatures as in the current system. For the case present in figures 3.14a and 3.14b the needed cooling power is 11 and 52 kW respectively. Additionally, the problems of holding a desired temperature for different configurations and the massive cooling required by the probe cooling systems are not solved. Moreover, part of the probe system that runs through the subsequent water quench cools the flow so fast so that all alkali condense there at the latest.

3.5.4 Probe exterior insulation

An improved isolation of the probe outer hull decreases the heat transfer rate into the probe system and allows the cooling oil to be replaced with pressurized air. This in turn makes the controlled quenching of the probe mass flow into the desired temperature range possible. A sketch of the principle is shown in figure 3.15.

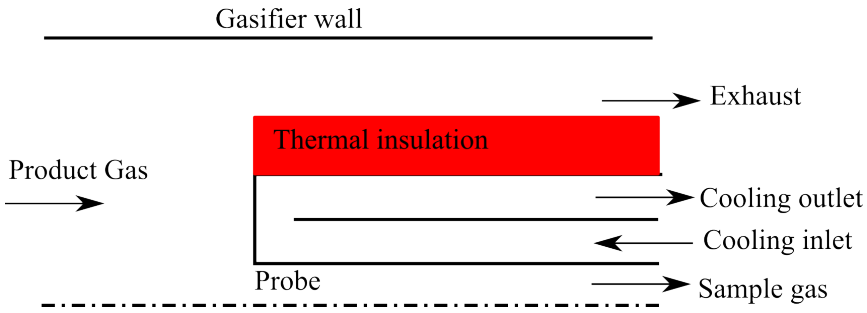

Figure 3.15: Principle of insulation of the probe system

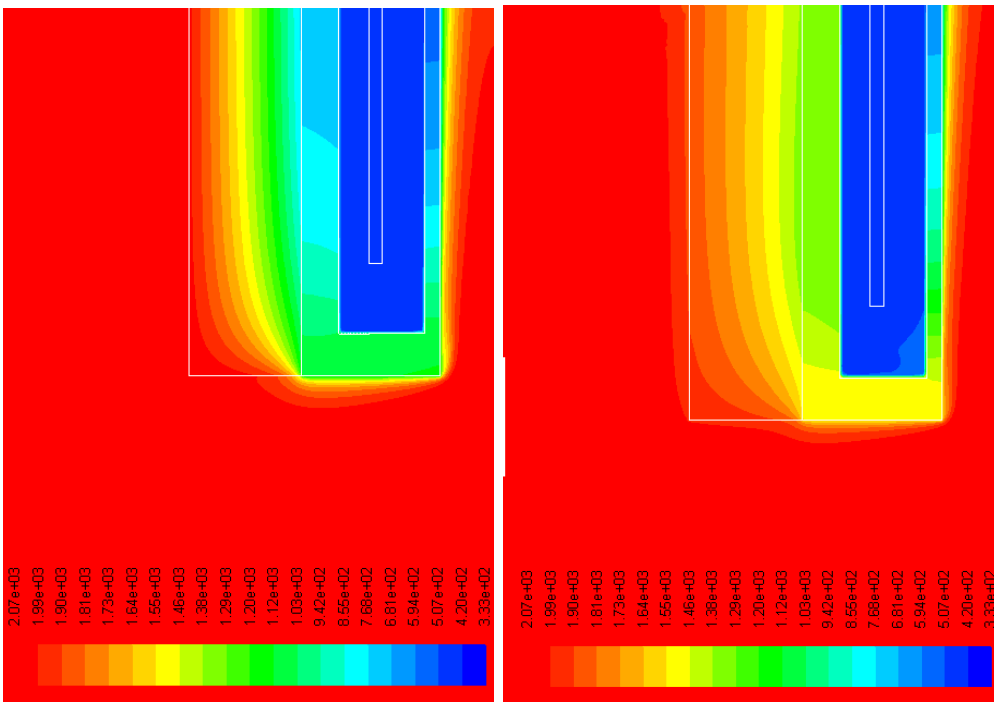

(a) **(b)**

Figure 3.16: Thermal distribution for the insulated cooling probe for (a) 100 mm and (b) 1100 mm exposure at 1800 °C

The needed cooling power for the cases shown in figures 3.16a and 3.16b are 2.7 and 42.2 kW, making an operation under the highest temperatures impossible. This approach would extend the operating conditions of the current system but the problem of trace component condensation remains unsolved. Moreover, the construction of a ceramic insulation around the probe is problematic for reasons of different heat expansion coefficients for steel and ceramic. As the principle of the insulation of the probe system interior, the needed insulation breaks the geometric and cooling power constraints of the gasifier tube. Furthermore, an

uniform temperature distribution on the inside pipe of the probe is not possible to produce without heating.

3.5.5 Rapid acceleration of the probe mass flow

This principle is based on the idea of pumping the probe mass flow rapidly out of the gasifier and through the quench water, thereby giving the mass flow too little time to cool down. Figure 3.17 shows the principle.

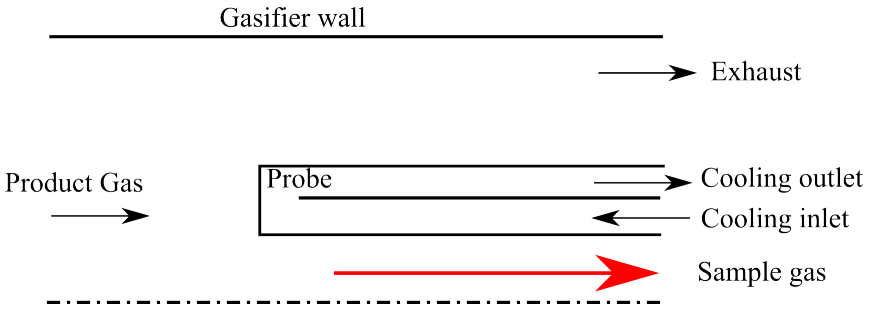

Figure 3.17: Principle of the rapid acceleration of the sample gas flow

This principle is rejected after the first test runs in Fluent because the required mass flow is higher than the main mass flow, making this approach unrealistic. Furthermore, the problem of massive cooling power is still present with this principle.

3.5.6 Internal heating of the analyzed mass flow

This principle is an enhanced version of the internal insulation principle. On the inner side of the inner insulations a heating element is installed which holds the temperature of the probe mass flow in the desired range, preventing condensation and slowing down the rate of reaction. This design is by far the most complex considering the small dimensions involved. Figure 3.18 gives an overview of this approach and figures 3.19a and 3.19b show the thermal distribution at 100 mm and 1100 mm exposure to the gasifier wall respectively.

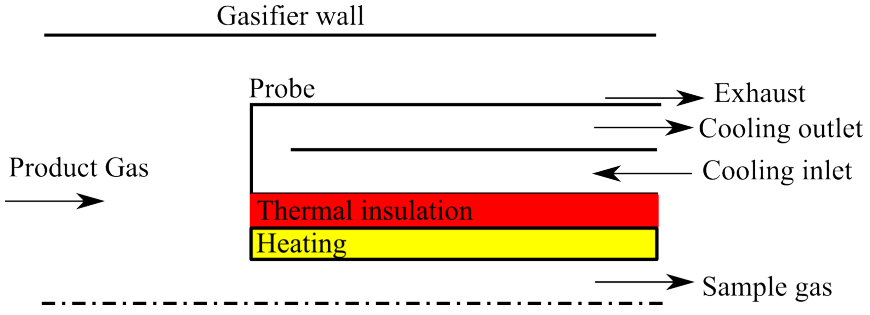

Figure 3.18: Principle of heating of the sample gas flow

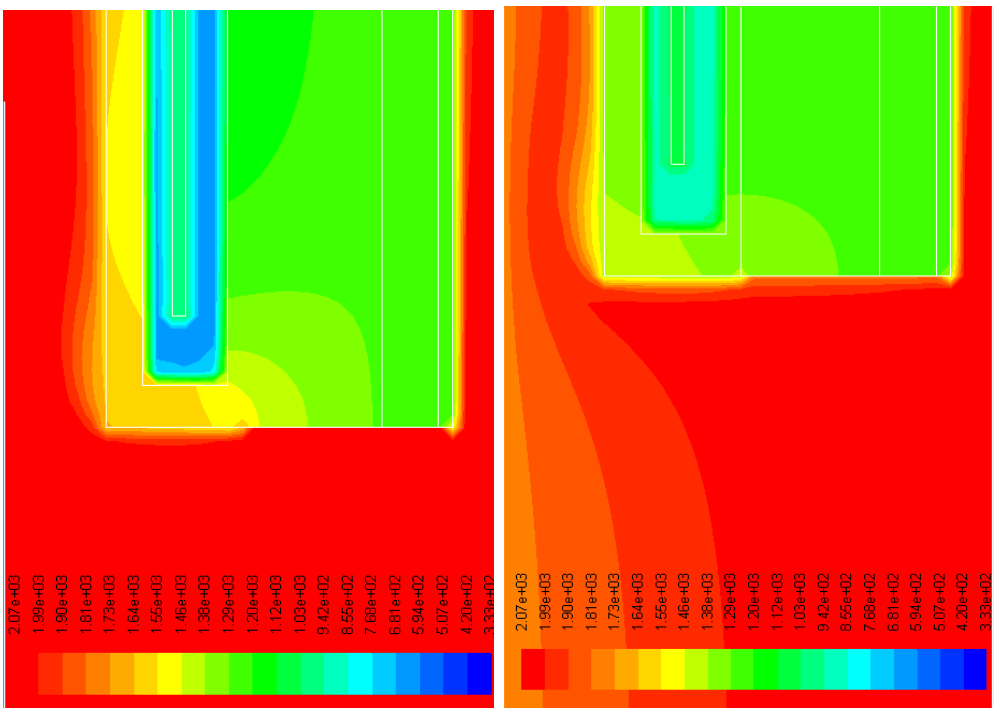

Figure 3.19: Thermal distribution for the heating probe for (a) 100 mm and (b) 1100 mm exposure at 1800 °C

The needed cooling power for the cases in figure 3.19a and 3.19b are 52 kW and 113 kW respectively. The probe temperature is significantly higher than in the current system even for 100 mm exposure length. It appears that the main heating power is cooled away by the probe cooling system, thereby nullifying the effect of the heating elements. An insulation between cooling and heating breaks the geometric constraints of the gasifier.

3.5.7 Focused condensation in a porous material

This principle tries to condense the trace materials in a controlled manner in a defined getter. This getter is later analyzed, allowing conclusions about the composition of the product gas at the position of sampling. As any condensation outside the gasifier has the problem of providing unaltered product gas, the defined condensation has to happen at the reaction stage to be analyzed. This rapid quenching is provided by mixing the product gas with cold flush gas. A sketch of this principle is shown in figure 3.20.

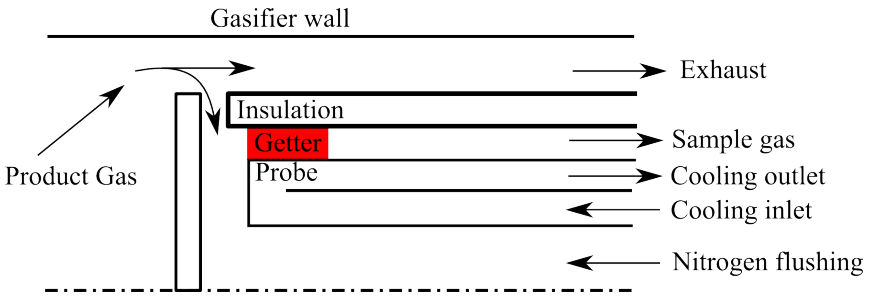

Figure 3.20: Marshmallow principle

A ceramic tube is placed around the cooled probe and flush gas pumped through the inner side of the cooled probe. The flush gas is pumped out of the probe system through the channel between the cooling probe and the ceramic insulation. When the mass flow pumped out of the system exceeds the flush gas mass flow, product gas is sucked into the probe system and mixes with the flush gas, leading to a rapid cooling of the product gas. The mixing temperature can be controlled by varying the ratio of flush gas to product gas in the system. In the gap between the cooling probe and the ceramic insulation a getter material is placed, providing sufficient surface area for condensation to appear. After measurements are made, the sample getter can be retrieved and analyzed. The temperature distribution at the probe tip for this principle is found in figure 3.21.

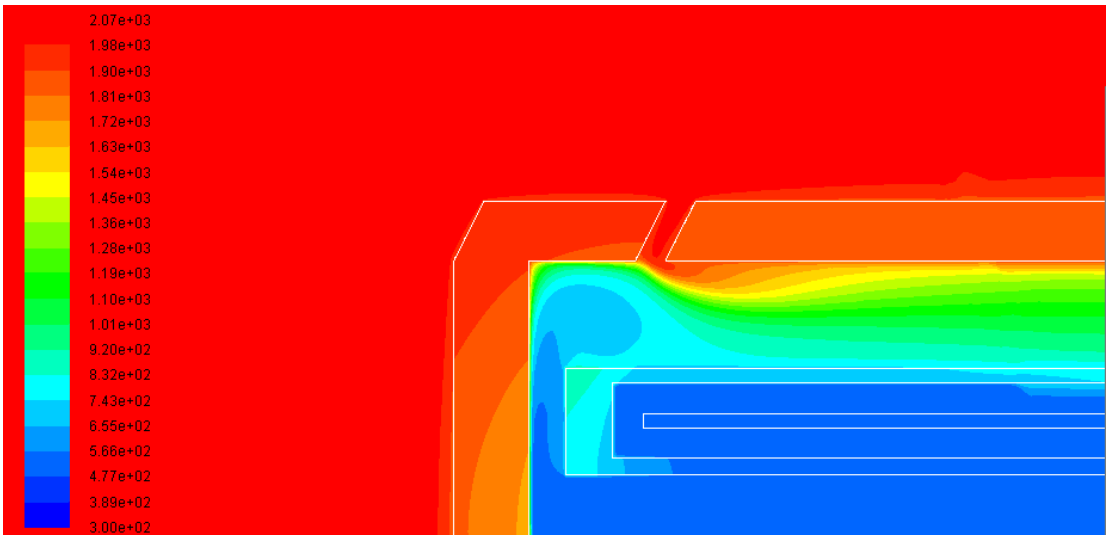

Figure 3.21: Temperature distribution at probe tip for the marshmallow principle

The temperature after the sample intake, when flush and product gas mix is significantly lower than the product gas temperature. The getter is placed directly after the product gas intake so that the rapid quenching happens in it, leading to condensation of trace materials in the getter.

Chapter 4

Construction

The principle based on defined condensation is chosen to be the most promising. To evaluate if the principle is applicable to lab conditions, an estimate of the measurement time is calculated. If the sampling time is too long to obtain data within a reasonable amount of time, the principle would not be viable.

4.1 Sample probe system

The sample probe system is constructed using Catia from Dassault Systemes and the parts it consists of are bought from multiple suppliers. (All order forms can be found in the appendix under section A.) A main aim is to enable the operator to change the getter during operation and without the danger of coming into contact with the hot gas. This is solved by installing the getter on the top of the cooling probe and pulling the whole cooling probe out of the measurement system while continuing to flush cooling into the ceramic. When the probe has passed the safety valve, it is closed and the operator can change the getter. Figure 4.1 shows the sketch and figure 4.2 the whole system.

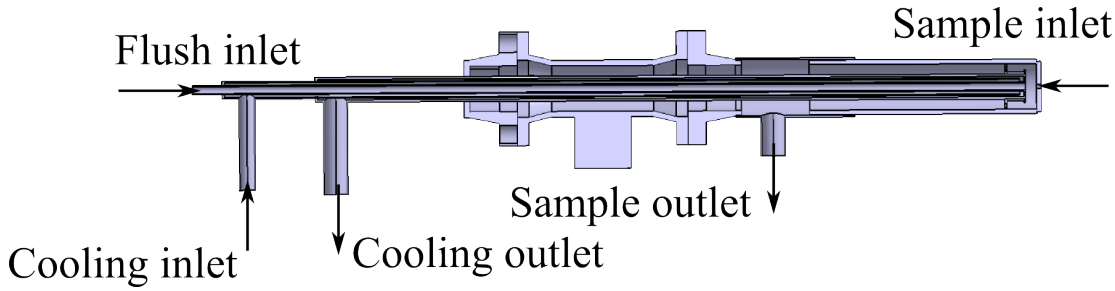

Figure 4.1: Sketch of sample probe system

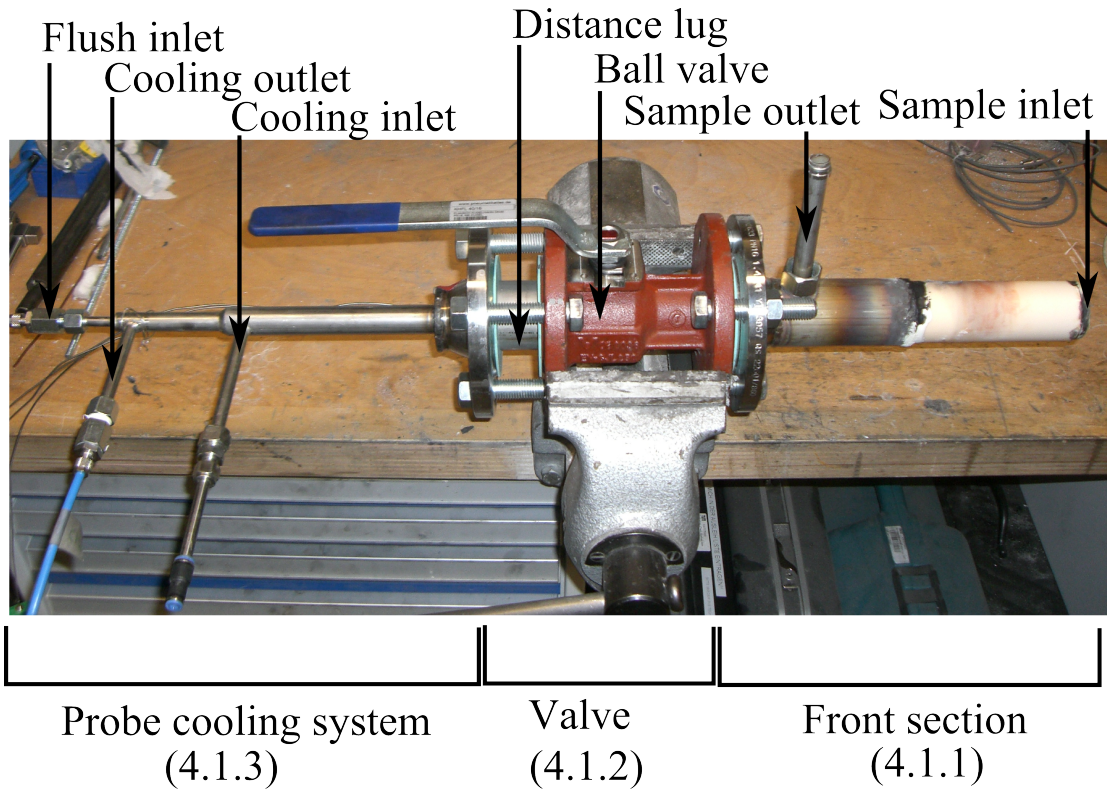

Figure 4.2: Constructed system with annotations

From the left the flush mass flow is pumped into the probe system. The inlet and outlet for probe cooling are interchangeable. Between the back section and the valve a distance lug is placed to vary the axial position of the probe tip in the probe system. The front section holds the sample in- and outlet. The whole verification system consists of the sample probe system, a tube furnace and some piping to provide cooling water and air to the system. An overview of the piping is found in figure 4.3.

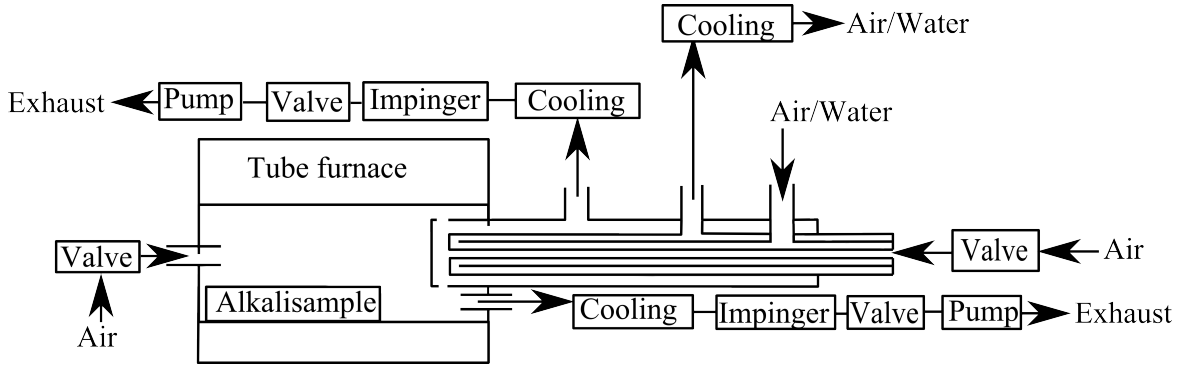

Figure 4.3: Piping and Instrumentation Diagram

The air mass flow entering the tube furnace through the main inlet can be varied by a volume flow meter. The order form for some of the volume flow meters and the range of the flow meters used in this work can be found in appendix A.12 and table 4.1.

4.1.1 Front section

Resulting directly from the need to insulate the flush mass flow from the tube furnace and the thermal stresses induced by the high temperatures in it, the outer hull of the sample retrieval system has to be made of ceramic, in this case bought from Friatec ceramics. The valve muff is a standard muff after DIN2633(PIN16) with a diameter of 40 mm. Onto this muff a steel tube with an inner diameter of 50 mm and 150 mm length is welded. The ceramic part consists of a tube and a ceramic disc with a hole in the middle. The resulting piece is glued into the valve muff. A high temperature ceramic glue bought for this experiment shows better performance than the ceramic glue present at the start of construction as this one does not have the necessary strength at temperatures exceeding 1400°C. When even higher temperatures are set in the experiments, even this glue fails and the disc falls off the ceramic tube. For the condensation experiment however, this has relevant effect as no particles have to be removed from the flow and a sufficient distance from the hot flow is achieved by placing the whole cooling probe further downstream in the ceramic insulation. A construction drawing, a sketch and the constructed part are found in figure 4.4.

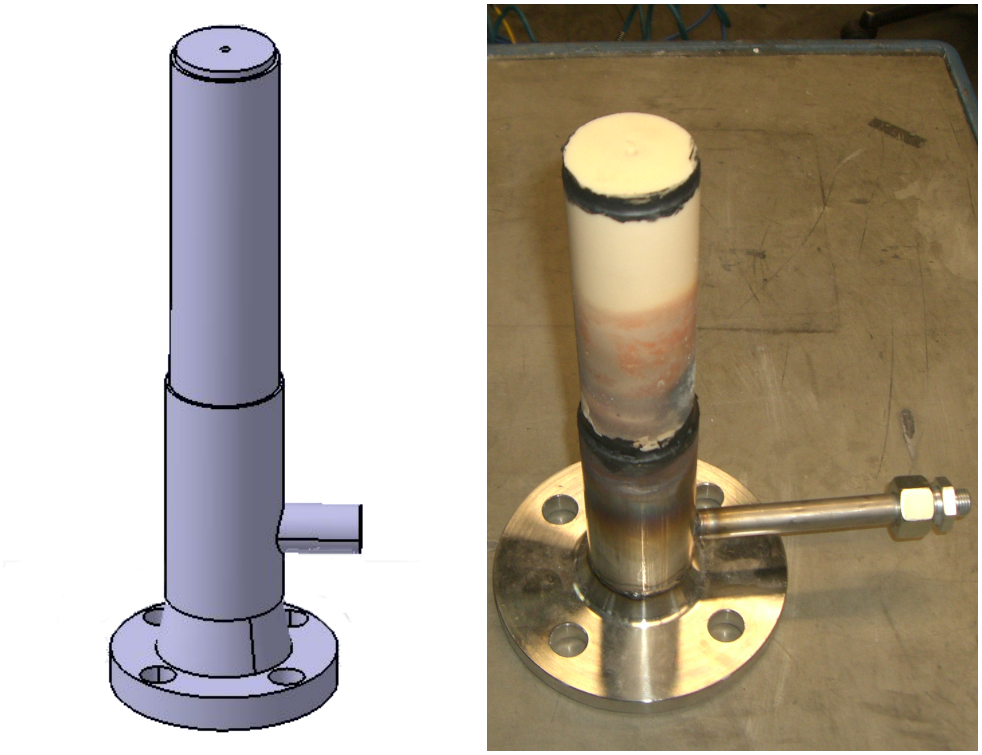

(a) (b)

Figure 4.4: Front section of measurement system: (a) Model of ceramic connection, (b) Constructed part

4.1.2 Valve

The safety valve protects the user from hot gas while the probe with getter cage is manipulated. It is also the part of the probe system that is installed in the system holder. The front and back section of the sample retrieval system are screwed to it, with seal rings in between to ensure airtightness. The valve is a ball valve with a cross section of 40mm, manufactured by the firm ESSKA. (The order form is found in the Appendix under figure A.7.) Muffs are installed on either side, the front muff holds the adaptor for the ceramic insulation and the sample flow outlet. The back muff is welded to the cooling probe system. Figure 4.5 shows a photo of the valve.

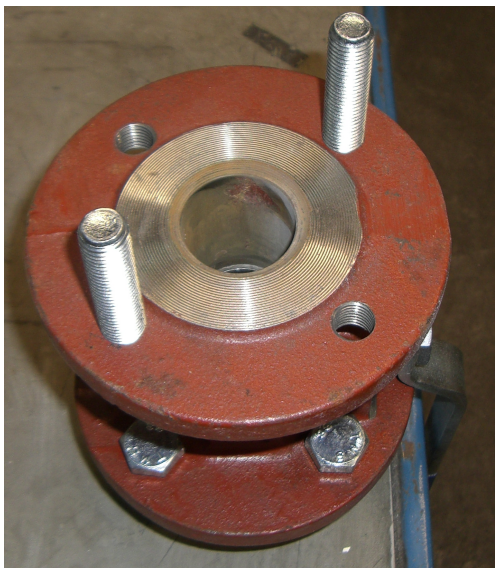

Figure 4.5: Valve for the sampling probe system

The screws are installed from the other side of the muff, the lever to open and close the valve can be seen on the right.

4.1.3 Probe cooling system

The probe system consists of the air cooled probe and the cooling flush. The cooling system consists of three pipes that are welded together in a fashion that allows an oil, water or air flow to the tip of of the probe in the inner tube, and back through the outer. That way, the returning cooling flow acts as insulation for the inner flow and the cooling flush flow. To finish construction, the rear muff to the safety valve is welded to it. It is also carrier for the temperature measurement system and the getter cage. Figure 4.6 shows the Catia sketch and the constructed part.

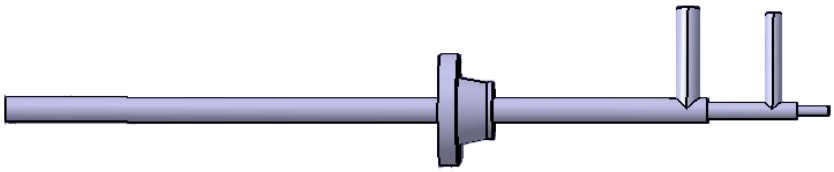

(a)

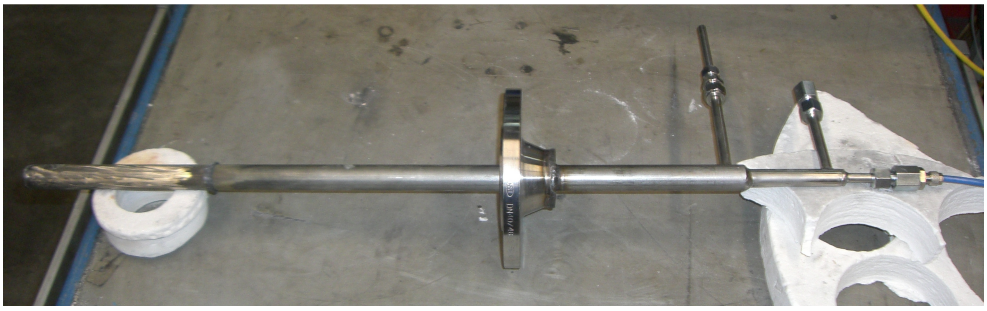

(b)

Figure 4.6: Cooling probe with connections for cooling and flush mass flow: (a) Model of cooling probe, (b) Constructed part

The first two pipes of the cooling system are for the cooling medium, the one at the far right for the flushing or sampling mass flow. The temperature sensors are put through small holes that are in the valve muff.

4.1.4 Sample getter

To place the sample getter for the marshmallow principle at the tip of the probe, two metal discs are put on the probe tip with a tight fit. The getter material is made out of insulation wool of the brand Alsitra. Figure 4.7 shows a sketch of the principle.

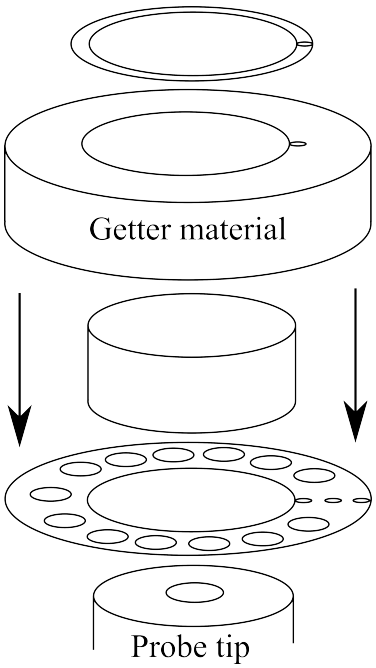

Figure 4.7: Sketch of sample getter for the marshmallow principle

The first experiments show that the volume of condensation is larger than could be covered by one layer of insulation cotton. Thus, the marshmallow is altered to 7 layers of Alsitra as sample getter. The sizing of the getter is done to match the length of condensation on the probe. Figure A.14 shows the colouring and the altered sample getter.

During the verification experiments, a variant called plug is built that uses a slightly altered position of the sample getter and changed flush and sample gas flows. A sketch of the principle can be found in figure 4.8 and a photo of the plug is shown in figure 5.9.

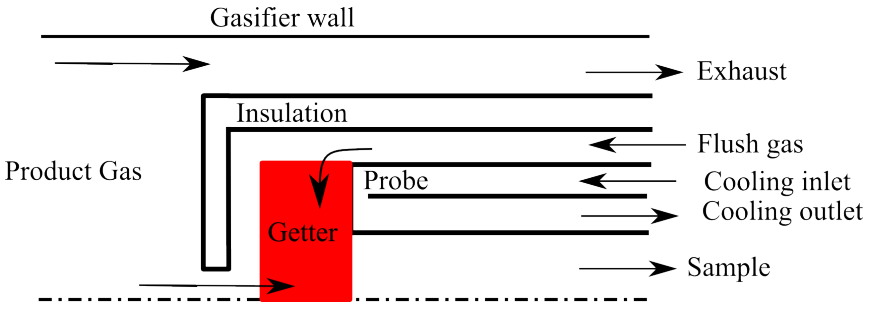

Figure 4.8: Plug principle

The sample getter is placed on the tip of the cooling probe, and the flush gas is pumped through the gap between ceramic tube and cooling probe. The sample mass flow is sucked through the sample getter and out of the measurement system. This way, the size of the condensation area is further reduced.

Another variant of the sample getter is the crown tip, where a metal plate is cooled by the flush gas so that trace components in the main flow condense on it. Figure 4.9 shows the overall principle. Notably, the cooling of the product gas is not the first coal of the flush gas, but cooling of the plate on which the trace components condense.

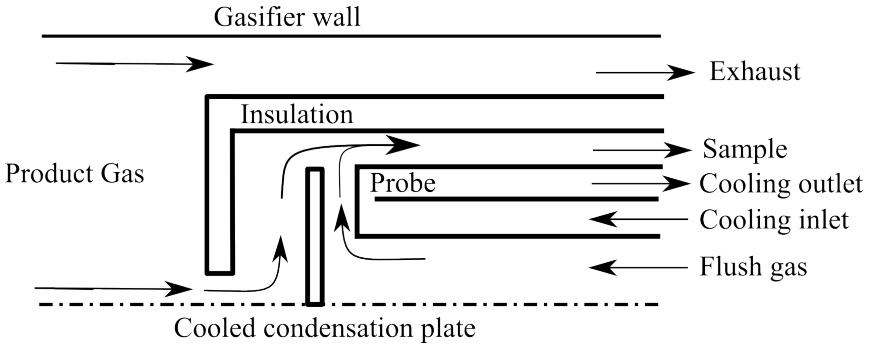

Figure 4.9: Sketch of crown principle

After the experiments, the condensed material is removed from the surface of the metal plate and analyzed via EDX. Figures 5.8a and 5.8b show the crown before and after exposure to sodium chloride at 1400 °C respectively.

4.1.5 Temperature sensors

The platform on which the getter is installed has four mount points for temperature sensors, which run down the probe gas shell and exit the system at the end of the probe. They enable temperature data of the cooling mass flow, the hot gas flow, the temperature in the mixing zone and the probe gas flow after the getter to be measured. The temperature sensors are type K thermo elements from TCDirect. Data logging is conducted using a four channel data logger which can be connected to the PC via USB. The order for the temperature measurement system can be found in Appendix A.13. The temperature is measured at four different positions, three of them located at the tip of the probe, one with varying penetration lengths around the cooling probe. The position of the temperature sensors is shown in figure 4.10.

4.1.6 Piping

The mass flow for the sample gas flow and the flushing are controlled with a Mass flow controller (MFC) having a value range between 4 and 40 l/h. Exhaust and main inlet flow are controlled with MFCs covering a range of 20-150 l/h. The exhaust and sample gas flow are first led through cooling tubes 4.11a, then washed in washing bottles 4.11b and exhausted via the MFCs after passing the vacuum pumps.

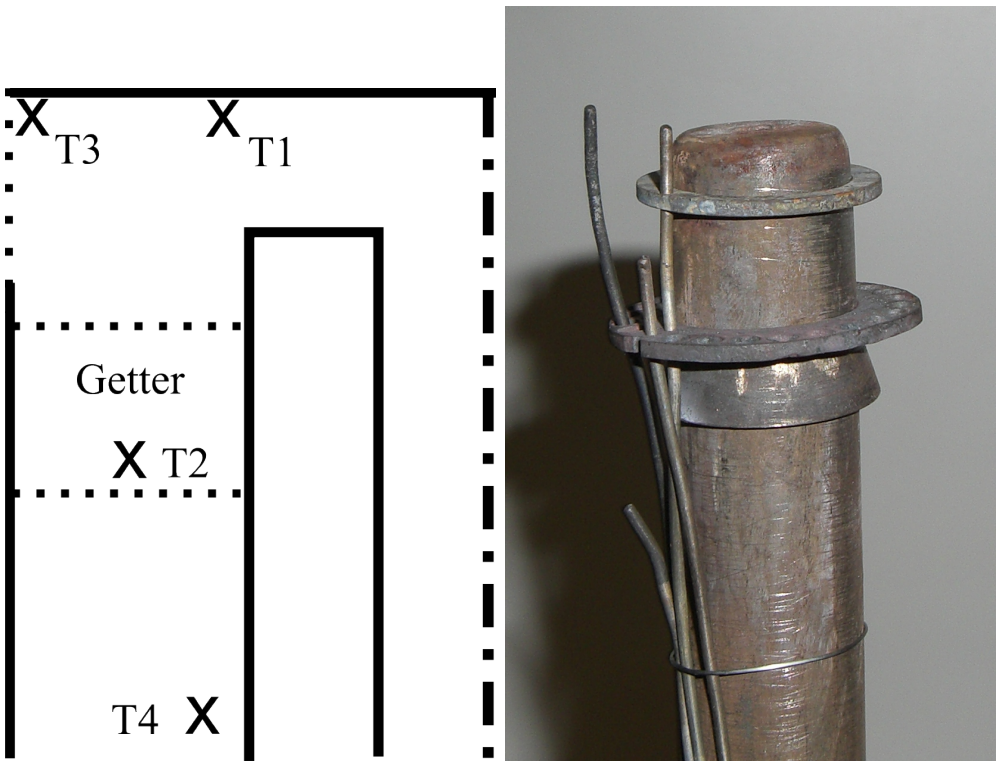

(a) (b)

Figure 4.10: Placement of temperature sensors, T_1 placed in the flush flow, T_2 in the getter, T_3 in the sample gas flow and T_4 downstream of the cooling tip: (a) Sketch, (b) Constructed Part

(a) (b)

Figure 4.11: Photos of the (a) cooling tubes directly after the tube furnace and (b) impingers to protect the MFCs from alkali vapor

Cooling of the probe happens via water cooling. Figure 4.3 gives an overview over the

piping of the measurement system. The water flow rate is controlled by measuring the time until one liter bottle is filled up. Depending on the tube furnace temperature, a flow rate between 15-40 $^{g}/_{s}$ is set. As the present volume flows are not sufficient to make an impact on overall temperature, the volume flow meters are replaced by the volume flow meters described in table 4.1.

Table 4.1: Volume flow meters of each flow

Flow	Range
Inlet	282-1410 $^{l}/_{h}$
Exhaust flow	282-1410 $^{l}/_{h}$
Cooling flush	60-240 $^{l}/_{h}$
Sample flow	60-240 $^{l}/_{h}$

However, due to a unit conversion error between the volume flows used in the simulations and the ones in the experiments, the volume flows are severely lower than the ones simulated so that experimental verification of the simulations is not possible. A simulation of the real experiment is found in the discussion in section 5.2.

4.2 Calibration of RFA

In order to make quantitative statements about the sodium chloride condensed in the samples, the RöntgenFloureszenzAnalyse (RFA) system (called by the english description EDX from now on) used needs to be calibrated. This happens by measuring the intensity of the K_α line of sodium for samples that are doted with 0.5, 1.0, 2.0, 5.0, and 10.0 mass % sodium chloride respectively. Figure 4.12a shows the milled insulation material in a mortar and figure 4.12b the pill that is manufactured out of the insulation material and wax.

(a) (b)

Figure 4.12: (a) Milled insulation material and (b) pressed pill ready for examination

With the intensity data it is possible to create a calibration curve. The curve is then used to interpret intensity data obtained from samples from the tube furnace experiments. Unfortunately, the florouscence of sodium lacks intensity to obtain quantitative results from the EDX as can be seen in figure 4.13a. To be able to get quantitative data, the direct correlation between the sodium and chlorine content is utilized. This is possible because sodium chloride is present as a molecule in the gaseous phase and the maximum temperatures of the experiments are below the point of thermic dissociation. Chlorine can be measured with far higher accuracy due to its higher relative intensity.

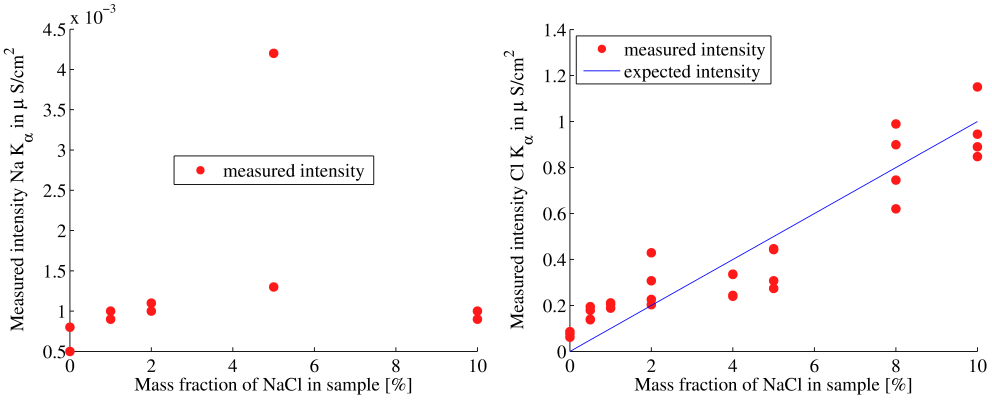

(a) (b)

Figure 4.13: Intensity of: (a) sodium K_α, (b) chlorine K_α florouscence over mass % sodium chloride in calibration samples

The intensity of sodium is ranging from 0.5 to $4.5 \cdot 10^{-3} \mu S/cm^2$, which is the lower detec-

tion limit of the EDX. As can be seen in the figure, the intensity does not change with the sodium chloride content in the calibration samples or varies wildly, making a calibration for quantitative measurement impossible. While the intensity of chlorine is measurable, as opposing to the sodium intensity, overall intensity is quite small which leads to a high range of error when it comes to quantitative measuring. Intensities for the same pill show also great variance if the pill is moved in between measurements. Two ways to improve homogeneity of the samples were tried: Solving the alkali chloride in distilled water, blending the mix with the insulation material and evaporating the water and pressing the remaining material to a pill, or pressing and milling the insulation material with salt repeatedly before adding wax to produce the pill for examination. Both approaches yielded similar results to the first, simple approach.

The measured intensities of chloride for experimental samples are very low. To ensure that different sample carriers and turret positions do not influence the intensity stronger than a different chloride content in the sample does, the 10% sample is measured in all eight different sample carriers at turret position 1 and in turret positions 1,2,4,8 and 16 using the same sample carrier. The results are shown in tabular 4.2 and 4.3 respectively.

Table 4.2: Measured intensities of chlorine and potassium in an 10 mass%-doted sample in different sample holders

Sample holder	Cl-intensity in $\mu S/cm^2$	K-intensity in $\mu S/cm^2$
1	1.25	1.3
2	1.19	1.24
3	1.31	1.34
4	1.2	1.26
5	1.26	1.29
6	1.26	1.29
7	1.18	1.23
8	1.26	1.29
Avg	1.24	1.28
Var	0.03	0.03

Table 4.3: Measured intensities of chloride and potassium in an 10 mass%-doted sample in different turret positions

Turret Position	Cl-intensity in $^{\mu S}/_{cm}$	K-intensity in $^{\mu S}/_{cm}$
1	1.25	1.302
2	1.267	1.297
4	1.226	1.267
8	1.215	1.274
16	1.206	1.287
Avg	1.232	1.28
Var	0.02	0.018

The influence of turret positions and sample holder is about 2 % of the base signal. While this is sufficiently precise for the doted samples, the samples taken from the experiment have lower sodium chloride contents so that no quantitative data can be obtained. Figures 4.13a and 4.13b show the intensity of sodium and chlorine over the mass % of sodium chloride in the calibration samples.

Chapter 5

Experiments

The experiments are used to verify the simulations and to investigate if the principle of defined condensation works in reality. A series of experiments is conducted:

- temperature measurements at different furnace temperatures and mixing ratios to compare to the simulations
- temperature measurements at different furnace temperatures along the cooled probe to asses the cooling power of the cooled probe
- condensation experiments with the marshmallow getter
- condensation experiments with the crown getter
- condensation experiments with the plug getter

5.1 Experimental setup

The tube furnace has to be manually controlled until the furnace temperature is over 300 °C because the type K thermocouples only deliver reliable temperatures above this temperature. Therefore, the controller of the tube furnace is set that the displayed heating current is always in the range of 15 to 20 Ampere. When the tube furnace temperature exceeds 300 °C, the automatic power control is activated and the furnace is heated up with a constant gradient of 3 $^{K}/_{s}$. To avoid thermal shocks in the probe system, the front section is installed in the tube furnace from the start. Before the cooled probe can be inserted into the probe system, the cooling has to be activated. After the experiments, the tube furnace is cooled with the gradient of 3 $^{K}/_{s}$.

5.2 Error in volume flows

During the end of the experimental investigation of the temperature distribution, an error in the range of the flow meter was discovered. While all simulations are set up that a

main flow velocity of 1 $^{m}/_{s}$ is achieved, the ordered flow meters can only deliver flow rates of up to 0.1 $^{m}/_{s}$. This can explain the unexpectedly low influence of flow velocity on the temperature distribution along the probe and at the probe tip. Additionally, it makes new simulations for verification necessary. The tube furnace system is modeled according to the models and settings described and each mass flow changed to the mass flow that is found in the real system. As the flows are controlled by volume flow meters outside of the oven, the standard density of air (1.275 $^{kg}/_{m^3}$) is used as conversion factor from volume to mass flow rate. The mass flows used for the new verification simulations are shown in table 5.1.

Table 5.1: Mass flows in verification experiment

Flow	1 to 1 (in $^{g}/_{s}$)	1 to 2 (in $^{g}/_{s}$)	1 to 3 (in $^{g}/_{s}$)
Inlet	$9.44{\cdot}10^{-5}$	$9.44{\cdot}10^{-5}$	$9.44{\cdot}10^{-5}$
Exhaust	$7.315{\cdot}10^{-5}$	$7.315{\cdot}10^{-5}$	$7.315{\cdot}10^{-5}$
Flush	$2.125{\cdot}10^{-5}$	$4.25{\cdot}10^{-5}$	$6.375{\cdot}10^{-5}$
Sample	$4.25{\cdot}10^{-5}$	$6.375{\cdot}10^{-5}$	$8.5{\cdot}10^{-5}$

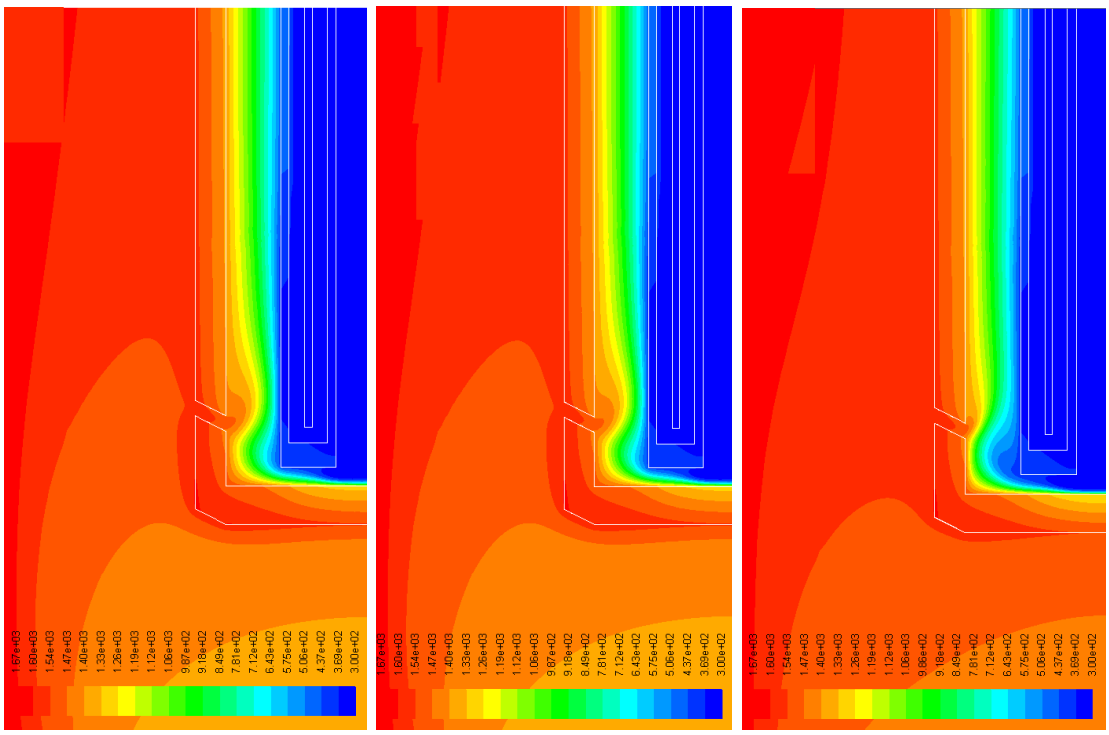

(a) **(b)** **(c)**

Figure 5.1: Temperature distribution with different mixing ratios: (a) 1 to 1, (b) 1 to 2, (c) 1to 3

Figure 5.1 shows the simulations corresponding to the real mass flows present in the temperature experiments. Due to the laminar flow in the probe system, the mixing of flush and product gas happens not as fast as expected. Thus, a high gradient in gas temperature in respect to position in the flow can be observed. Moreover, the temperature distribution in the probe system does not vary greatly with the mixing ratio. This can be attributed to the fact that the convective cooling of the probe is the dominating cooling effect in this system. Combined with difficulties in defining the position of the thermocouples in the experimental set-up, a verification of these calculations is hard to establish. All temperature and condensation experiments are carried out with the reduced mass flow, so a reduced effectiveness of flow mixing has to be anticipated.

5.3 Temperature measurements

To verify the effectiveness of the mixing of flush and sample flow, the tube furnace is heated to different temperatures, the cooling probe is fitted with thermocouples according to sketch 4.10 and installed in the measurement system. The temperatures analyzed range from 800 °C to 1400 °C in 100 °C steps. For each temperature, the mixing ratio

$$x = \frac{\dot{m}_{sample}}{\dot{m}_{sample} + \dot{m}_{flush}} \tag{5.1}$$

is varied. The aim is to find out how and where the mixing of flush and sample flow has a cooling effect and in which magnitude. For all experiments, the volume flow of the product gas into the probe system is 60 l/h for all ratios except 0 and 1, where the total sample volume flow is set to 240 l/h. The main inlet flow is 340 l/h and the exhaust 280 l/h. The thermocouples are of type K, having a range from -80 °C to +1300 °C for a short time. The probe is cooled with a water mass flow of 20 g/s. All temperature data is taken when no transient behavior is apparent.

5.3.1 Dependence on mixing ratio

To determine the influence of the mixing ratio on the probe tip temperature, several mixing ratios are set at different tube furnace temperatures. After each change in the mixing ratio, temperature data is taken as soon as the temperature shows no signs of transient behavior any longer. The simulated results are obtained by extracting the air temperature at the position of the thermocouples in the simulation. Figure 5.2 shows the results of the temperature measurements at the probe tip.

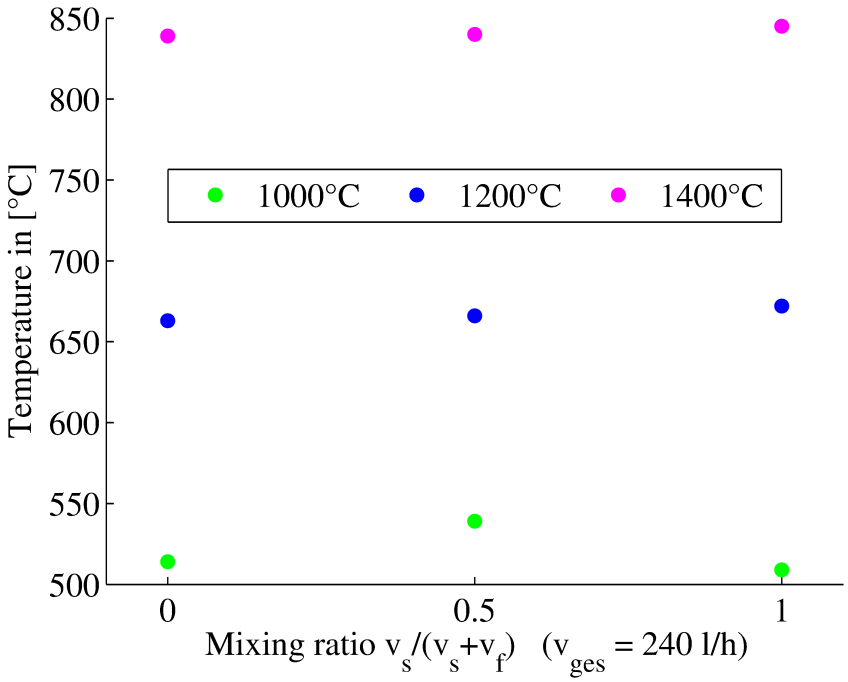

Figure 5.2: Temperature at probe tip over mixing ratio at different tube furnace temperatures

The temperature distributions show only a little temperature dependency on mixing ratio. Due to the very low velocity and Reynolds number, very little mixing occurs, so the temperature distribution in the sample gas channel is layered. This temperature measurement is more influenced by the position of the thermocouple than of the mixing ratio. Furthermore, the temperature measurement is further impaired by the convective cooling of the exhaust mass flow and radiation. In addition, the volume flows are too small for a temperature drop due to the mixing of flush and product mass flow.

5.3.2 Probe cooling

Three thermocouples are placed at the cooling probe tip, 10 and 20 cm downstream from the probe tip respectively. Thus, the first thermocouple is in the tube furnace, the next in the transition region between tube furnace and outside and the third at the height of the exhaust outlet. The mixing ratio x is left at 0.25 all the time. The temperature is increased from 800 °C to 1400 °C in 200 °C steps. Figure 5.3 shows the result of this experiment.

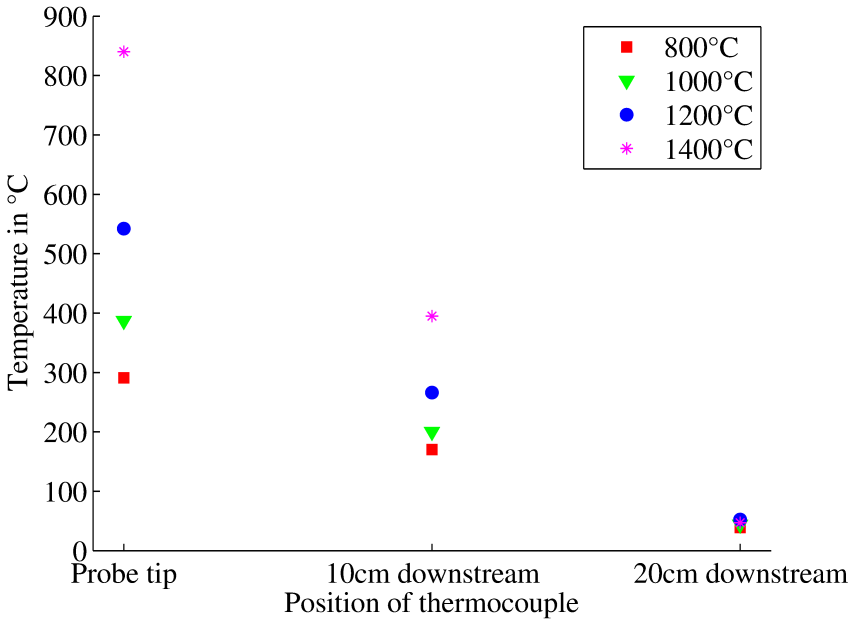

Figure 5.3: Dependence of temperature from probe cooling

The difference in probe temperature on tube furnace temperature is greatest at the probe tip and decreases fast further downstream. At the temperature sensor 20 cm from the probe tip, almost no influence of tube furnace temperature can be found. The water cooled probe cools the sample gas flow in with far greater power than the mixing ratio of flush and sample gas flow. The probe cools the air flow This can be attributed to the low air mass flows in the probe system so that the influence of the convective cooling of the probe is dominant.

5.4 Estimate of measurement operation

For a measurement of trace components through condensation, one has to ensure that sufficient trace materials are trapped in the sample getter to exceed the detection limit of the measurement method, in the present work a energy-dispersive X-ray spectroscop manufactured by Shimadzu. Following calibration efforts with the machine, it is assumed that results with sufficient resolution are possible if the amount of analyte condensed in the sample exceeds 1 mass %. With a sample weight of approximately 1 gram, one should get reasonable measurements if 0.01 gram of potassium or sodium chloride are condensed in the sample. The time of measurement can now be estimated using:

$$t_{measurement} = \frac{m_{sample} Y_{detect}}{Y_{sampleflow} \dot{m}_{productgas} Y_{analyte}} \tag{5.2}$$

with m_{sample} being the mass of the sample getter, Y_{detect} the detection limit of the measurement method, $Y_{sampleflow}$ the ratio of the sampling mass flow to the main mass flow, $\dot{m}_{productgas}$ and $Y_{analyte}$ the estimated mass fraction of the analyte in the product gas. Table 5.2 gives an overview of the estimates and the resulting measurement time to reach sufficient condensed analyte mass in the sample getter.

[t] Attribute	Value
m_{sample}	1g
Y_{detect}	0.01
$Y_{sampleflow}$	0.2
$\dot{m}_{productgas}$	1g/s
$Y_{analyte}$	1-100ppm
$t_{measurement}$	500-50000s

Table 5.2: Estimates for measurement conditions

The measurement times vary from 8 minutes to 14 hours, which is possible to operate in the lab. Variations in the other flow attributes can drastically lengthen or shorten measurement times, making them impossible. The estimates are only guidelines in which timespans the mass is condensed in detectable manner. Thus, defined condensation is viable for some coals with high alkali content in the untreated product gas.

5.5 Condensation experiments

For condensation experiments, the oven temperature is set to 1400 °C and a sample holder containing potassium chloride is inserted in the back side of the tube furnace, near the main air inlet. The sample holder is shown in figure 5.4. Based on the first temperature measurements, the flush gas flow is set to 0 l/h and the sample mass flow to 240 l/h. Then, 2 g of potassium chloride is inserted at the main inlet of the tube furnace. The carrier of the alkali is the sagger shown in figure 5.4.

Figure 5.4: Sample holder with molten and re solidified NaCl

The sagger is made of the same material as the insulation material and shows great temperature shock resistance. The chloride is evaporated after 20 minutes, resulting in substantial loading of the main flow shown in figure 5.5. After that, the cooling probe with sample getter is pulled out of the system and the getter material removed from the probe tip for analysis in the EDX. The cooling tube for the exhaust mass flow is severely corroded after all experiments. Figure 5.6 shows the tip of the exhaust cooling tube after all condensation experiments.

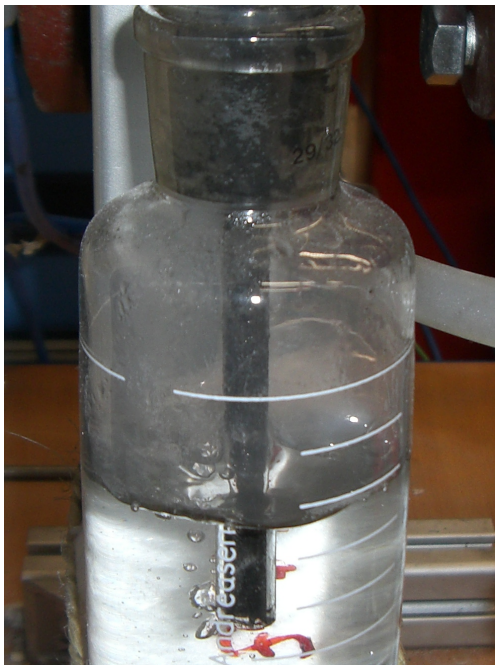

Figure 5.5: Vapor in the exhaust impinger during sodium chloride experiment

The vapor in the upper part of the impinger is the chloride loading after the exhaust flow has passed through the water, so the chloride loading in the tube furnace can be regarded as being very high.

Figure 5.6: Tip of the exhaust cooling tube after alkali chloride experiments

The exhaust pipe is heavily corroded after each experiment and all brittle material removed. The exhaust pipe thus shrank in length from experiment to experiment.

5.5.1 Marshmallow experiments

The marshmallow getter is installed on the probe tip and inserted into the probe system. It is exposed to 2 g of sodium chloride which is evaporated in 20 minutes at 1400 °C. The samples obtained are taken from the probe tip, milled and pressed into pills. The samples are compared to a blind sample. Because of the high mass of material at hand, two pills each are produced. Figure 5.7 shows the intensities of the samples.

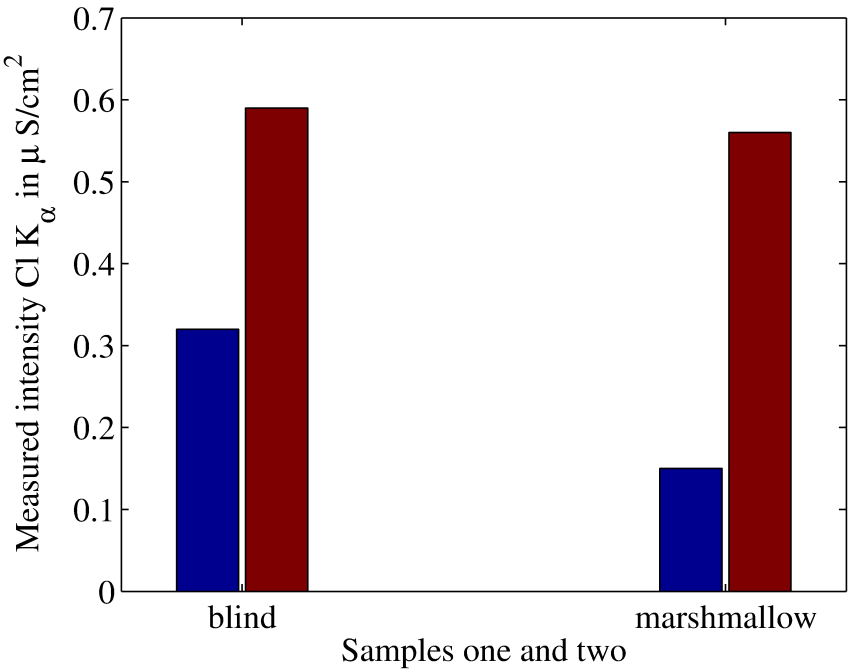

Figure 5.7: Cl intensities of different samples from the marshmallow experiment, two pills each

As can be seen, the intensities for the blind and experimentally obtained samples vary greatly, but are in the same range. No quantifiable change in getter composition can be confirmed, although the appearance of the sample getter changes from before and after the experiments, as can be seen in figures A.15a and A.15b. The samples show a clear colour change where they touch the cooling probe as can be seen in figure A.16.

5.5.2 Crown experiments

The crown tip is installed on the probe and inserted into the tube furnace. The flush gas flow is set to 180 l/h and the exhaust flow to 240 l/h. After 20 minutes of exposure to sodium chloride, the crown tip is taken out of the probe system. The crown plate is covered by a black, brittle material. Figures 5.8a and 5.8b show the crown tip before and after the experiment. This material is scratched from the surface of the plate and pressed into a pill. Although qualitative analysis confirms the presence of sodium and chlorine in the sample, no quantitative result different from background intensity is found.

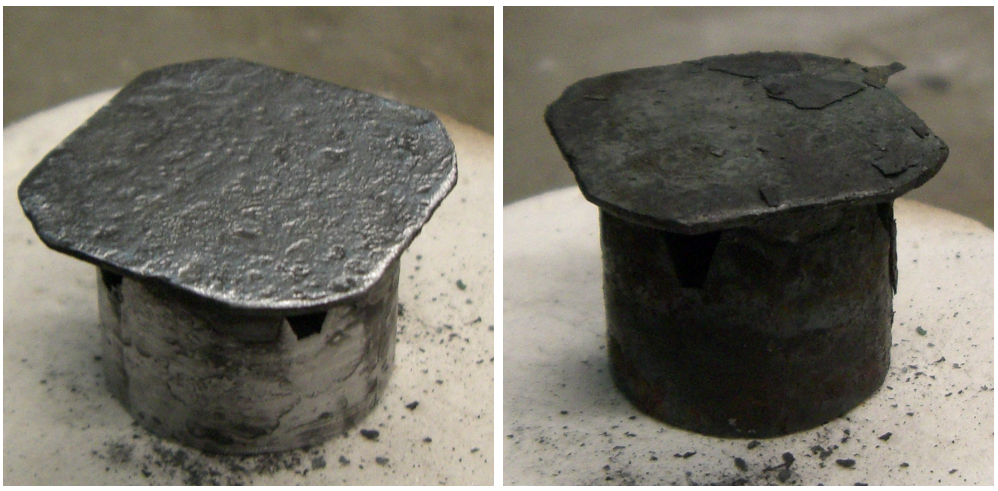

(a) (b)

Figure 5.8: Crown tip before and after experiments with sodium chloride: (a) Crown tip before experiment, (b) Crown tip after 20 minutes at 1400°C and sodium chloride

5.5.3 Plug measurements

The sample obtained with the plug system during an experiment is analyzed and compared with a blind sample and a blind sample that has been exposed to heat in the tube furnace without any evaporation of alkali in order to assess the effect of composition change in the sample getter material. Figure 5.10 shows the resulting intensities of the spectroscopic measurements. The plug holder is covered in the same black, brittle material after the experiments as the crown. The visual change over the experiment can be seen in figures 5.9a and 5.9b respectively.

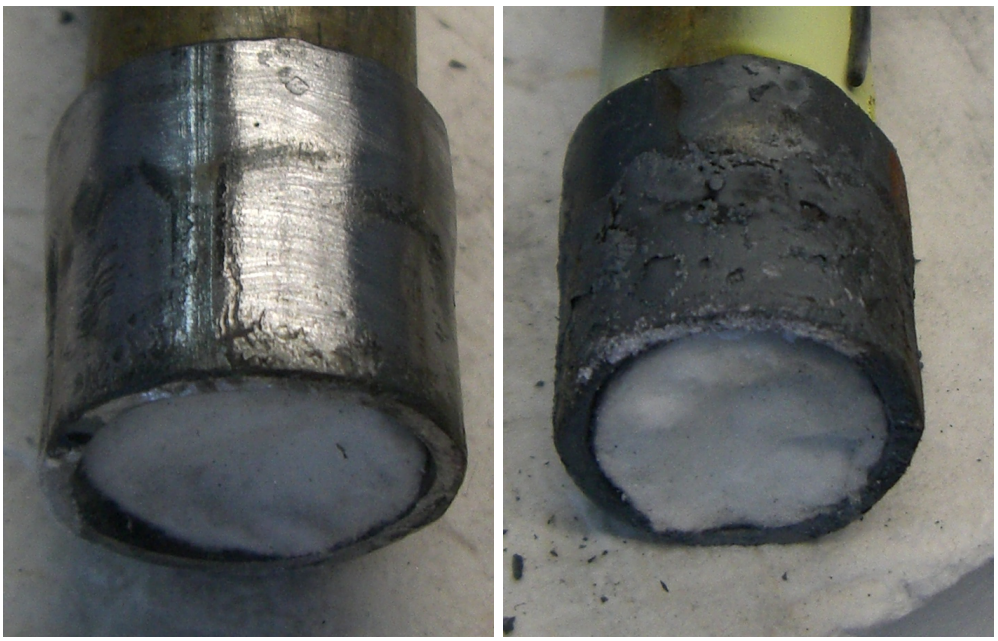

(a) (b)

Figure 5.9: Plug tip: (a) before and (b) after experiments with exposure to 2 g potassium chloride for 20 minutes at 1400 °C

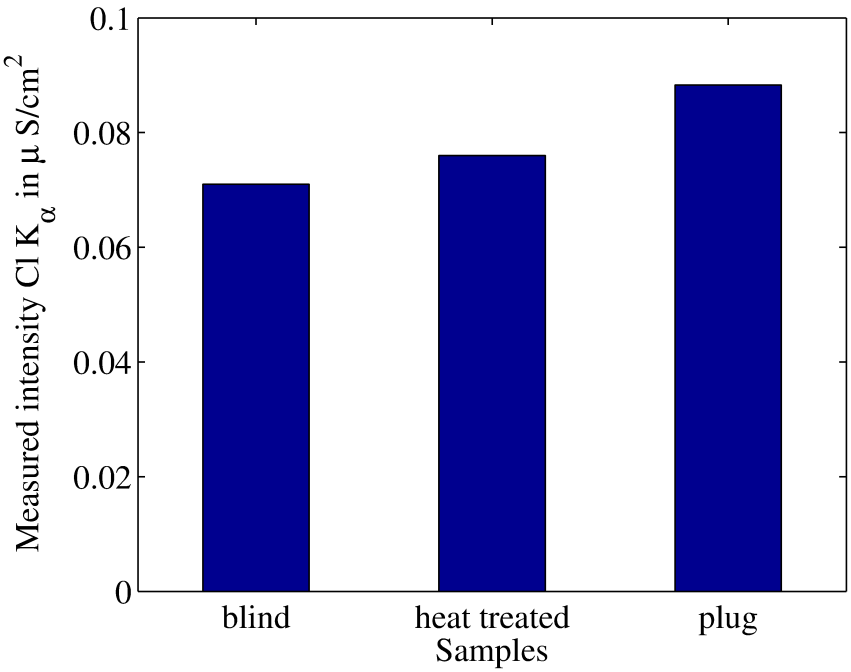

Figure 5.10: Cl intensities of different samples for the plug experiment

While the intensity of the sample from the experiment is higher than the blind and the treated sample, the measured increase in intensity compared to the background intensity of the blind sample is quite low. Therefore, drawing quantitative results from this experiment is not possible.

Chapter 6

Conclusions

6.1 Discussion

The temperatures obtained from the simulations show similar trends as the measurements in the verification, but the effect is not near as clear as in the simulations. Several factors and uncertainties contributed to this result. The simulations as well as the analytical approach used in the thesis by Donaubauer (2012) lacks crucial data on the radiation physics, material constants and great simplifications on the flow are made. Effects of a dust-laden and self absorbing gas flow are ignored. This makes results concerning the temperature and with it condensation points and heat flows inaccurate for the analytical as well as the numerical approach.

During the experiments it appears that the main influence factor on the temperature is the distance between the temperature sensor and the cooling probe. The mixing ratio of flush and sample mass flow is a minor influence. While a sufficient and reliable cooling of the probe is good in itself, it makes the verification of flush cooling at the probe tip improbable. Temperature trends obtained when changing mass flows and flush rations are smaller than expected and cannot be safely attributed to the mixing ratio, as convective cooling can also reduce the temperatures of the temperature sensors. Moreover, the ratio of mass flows involved are to low to have a significant effect on overall temperature in the tube furnace due to constant heating from the outside, and higher mass flow ratios would complicate their precise adjustment and further decrease the sample mass flow into the probe system.

A big issue in the experiment is the inability to create mass flows of sufficient magnitude, as the pumps and mass flow meters ordered have to little range to create the air flow velocity required. However, while higher mass flows would certainly have a higher impact on temperature trends, the hope that alkali chloride condensation in the sample getter would increase to distinctively measurable levels may be misguided. According to the measurement depicted in figure 5.7, the exposure to a sodium chloride atmosphere

yielded no increase in intensity. This can be attributed to the fact that too little sodium chloride condensed in the sample getter.

The alternative plug design showed an increase in intensity and therefore condensed material, but not substantial enough to draw conclusions from it. The alkali chlorides condense more in the insulation plugs connecting the probe system with the tube furnace and in the cooling tubes, corroding them over time.

The experiments show that the ansatz to condense the analyte in a distinct location does not have the desired magnitude, at least under the conditions tested in this project. While condensation is proven to happen in the vicinity of the probe tip, the mass of the condensed material is too low to yield any quantitative result from the EDX, even when the pure compound is evaporated in the tube furnace. In bigger applications, this could be balanced by taking samples for a long time, but for some modes of operation these times would be too long to be feasible in day to day lab conditions. When taking into account the weak intensities of the florouscence for sodium, potassium and chloride, one comes to the conclusion that a product gas analysis using this approach is not feasible with the conditions described in the introduction.

Furthermore, the correlation of sodium to chloride for a measurement via EDX is only valid if sodium chloride is evaporated. There is no such simple correlation for sodium bound in organic or in coals, sodium is bound in different compounds, which nullifies this approach. In summary, the approach of freezing the condition at sample intake via condensing is in principle very promising, but not realizable.

6.2 Simulation of subsequent probe system

A realizable principle is to use a ceramic probe to take samples in the reaction zone and cooling and retaining them to 1000 °C when the quench zone is reached. This does not stop the reaction in the ceramic part of the probe system but the system is able to take samples from every stage of the gasifier with ease, evading the cooling problem. The principle is shown in figure 6.1.

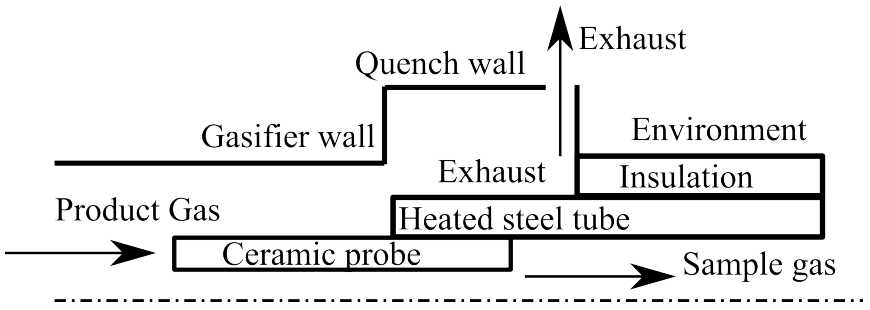

Figure 6.1: Principle of the ceramic probe for hot gas extraction

A ceramic tube is fit into a heated steel tube that is installed under the quench zone. The ceramic tube can be axially moved within the system, allowing for samples to be taken from the beginning to the end of the reaction zone. This heating system ensures that the ceramic tube does not suffer from thermal stress created by the high temperature gradient from the reaction zone to the quench and keeps the sample gas at 1000 °C until it enters a gas analyzer. An overview of the boundary conditions for the simulation is given in figure 6.2

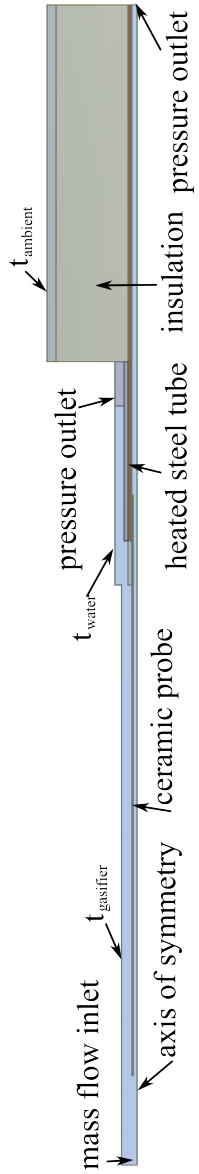

Figure 6.2: Boundary conditions for ceramic probe simulation

The system is simulated with the gasifier wall temperature set to 1800 °C and a total mass flow of 1 g/s. The ambient temperature is set to 27 °C and the insulation material has a mean heat conductivity of 0.5 W/mK. In the current design, the ceramic tube has a length of 1.1 m into the gasifier, which is simulated as a 1.3 m long tube. The quench zone is about 40 cm long, and the insulation material has a thickness of 15 cm. A first simulation shows that the required heating power is around 3 kW if the heating system is sufficiently

insulated. Figure 6.3 gives the temperature distribution in the ceramic probe system when the gasifier is heated to 1800 °C.

The ceramic tube has the same temperature as the main flow in the reaction zone, and retains the sample flow over 1000 °C throughout the quench until it passes out of the domain. The hot gas can then be sent to the gas analysis via a heated pipe.

Figure 6.3: Temperature distribution of subsequent probe system

Bibliography

Agilent Technologies (2005). *Inductively Coupled Plasma Mass Spectrometry*. Agilent Technologies.

Ansys (2012). Description of ansys fluent.

Antoine, C. (1888). Tensions des vapeurs; nouvelle relation entre les tensions et les températures.

Bläsing, M. and Müller, M. (2010). Mass spectrometric investigations on the release of inorganic species during gasification and combustion of rhenish lignite. *Fuel*, 89:2417–2424.

British Petroleum (2006). Statistical world review of world energy 2009. `www.bp.com/liveassets/bp_internet/globalbp/globalbp_uk_english/reports_and_publications/statistical_energy_review_2008/STAGING/local_assets/2009_downloads/statistical_review_of_world_energy_full_report_2009.xls#%27Primary`.

Donaubauer, P. (2012). Wärmetechnische Auslegung einer Probenahmelanze. Master's thesis, Technische Universität München.

Energy Information Association (2009). Energy intensity of different economies. `www.eia.doe.gov/pub/international/iealf/tablee1p.xls`.

Geisberger (2010). Konstruktion einer Partikelprobenahmesonde. Master's thesis, Technische Universität München.

Hauk, F. P. (2011). *Entwicklung einer Thermowaage zur Untersuchung des Alkaliverhaltens bei höchsten Dücken und Temperaturen*. PhD thesis, Technische Universität München.

Higman, C. and van der Burgt, M. (2003). *Gasification*. Gulf Professional Publishing.

International Monetary Fund (2012). Gross domestic product, worldwide. `www.imf.org/`.

makeitfrom.com (2013). Material properties of al2o3. `www.makeitfrom.com/material-data/?for=Alumina-Aluminum-Oxide-Al2O3`.

Müller, M. (2009). Freisetzung und einbindung von alkalimetallverbindungen in kohlebefeukohle kombikraftwerken. *Schriften des Forschungszentrums Jülich Reihe Energie und Umwelt*, 34.

Monkhouse, P. (2011). On-line spectroscopic and spectrometric methods for the determination of metal species in industrial processes. *Progress in Energy and Combustion Science*, 37(2):125 – 171.

NIST Webbook (2012). Phase change data for nacl and kcl. `webbook.nist.gov/chemistry/form-ser.html`.

Richter, H. (2008). Piter-zusammenbau-1338-2008-m-0-01. Technical report, Xerion Advanced Heating.

Spliethoff, H. (2010). *Power Generation from Solid Fuels*. Springer.

Spliethoff, H., Bottegi, F., Erbel, C., Gleis, S., Haselsteiner, T., Hauk, F., Kunze, C., Losurdo, M., Nakonz, M., Papadopoulos, T., Stetka, M., and Tremel, A. (2011). Hotvegas abschlussbericht. Technical report, Lehrstuhl für Energiesysteme.

Steffin, C. R. (1998). *Freisetzung und Einbindung von Alkalien bei der Verbrennung und Vergasung von Kohle unter Druck*. PhD thesis, Universität-Gesamthochschule Essen.

Stemmler, M. (2010). *Chemische Heißgasreinigung bei Biomassevergasungsprozessen*. PhD thesis, Technische Hochschule Aachen.

Voss, P. (2008). *Elementzusammensetzung der RWE-Einsatzkohlen (Projekt HotVeGas)*. RWE Power.

Appendix A

Appendix

A.1 CFD setup and Fluent settings

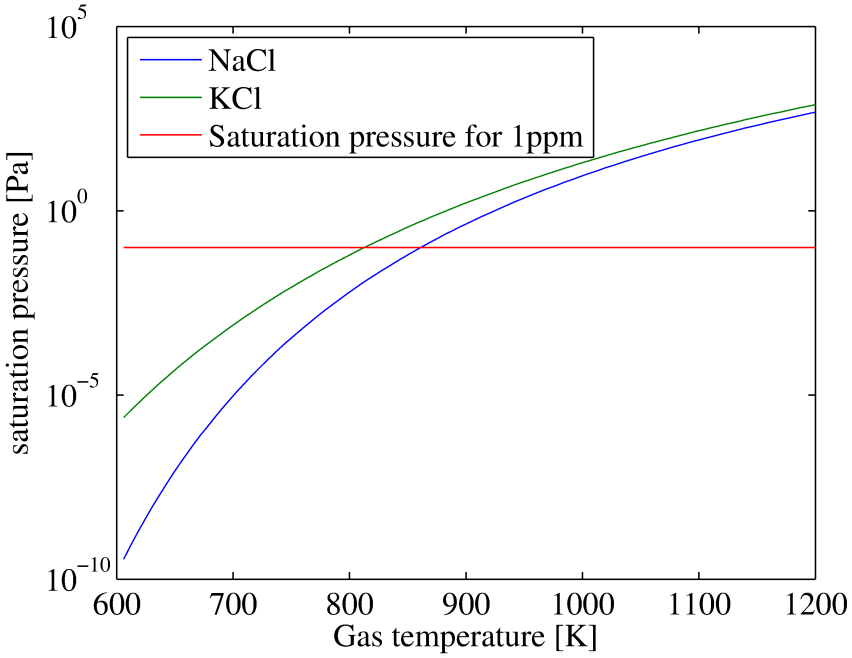

Figure A.1: Saturation pressures of KCl and NaCl over main flow temperature

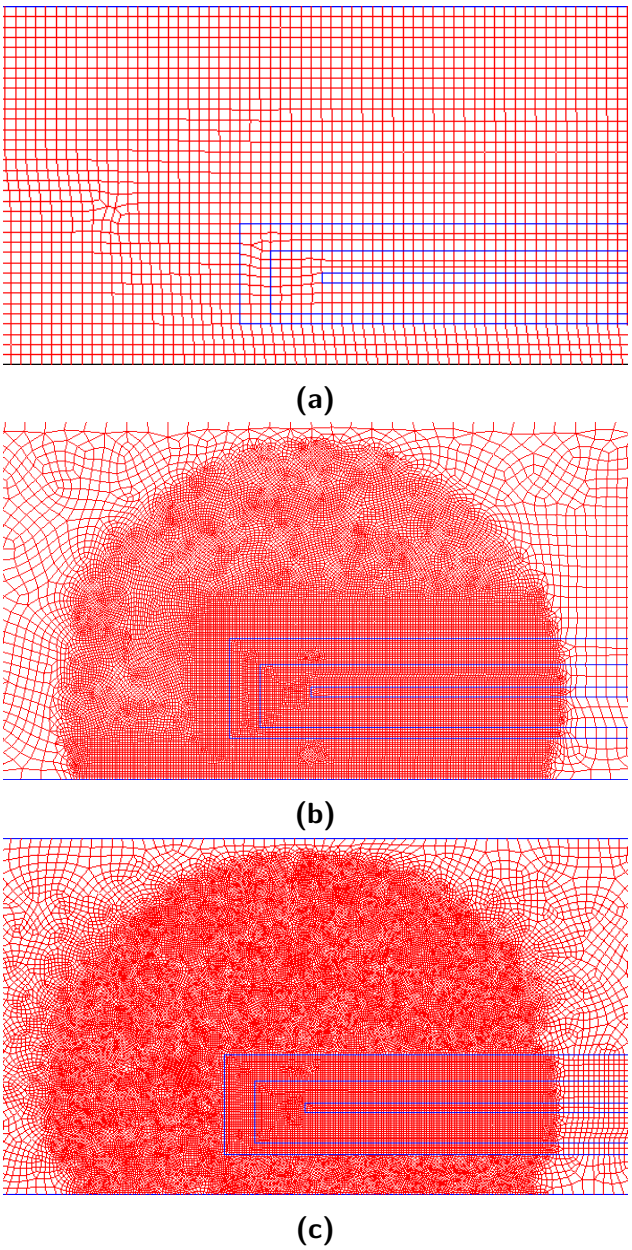

(a)

(b)

(c)

Figure A.2: Meshes of increasing cell number: (a) Rough mesh, (b) Standard mesh, (c) Fine mesh

A.2 Construction drawings

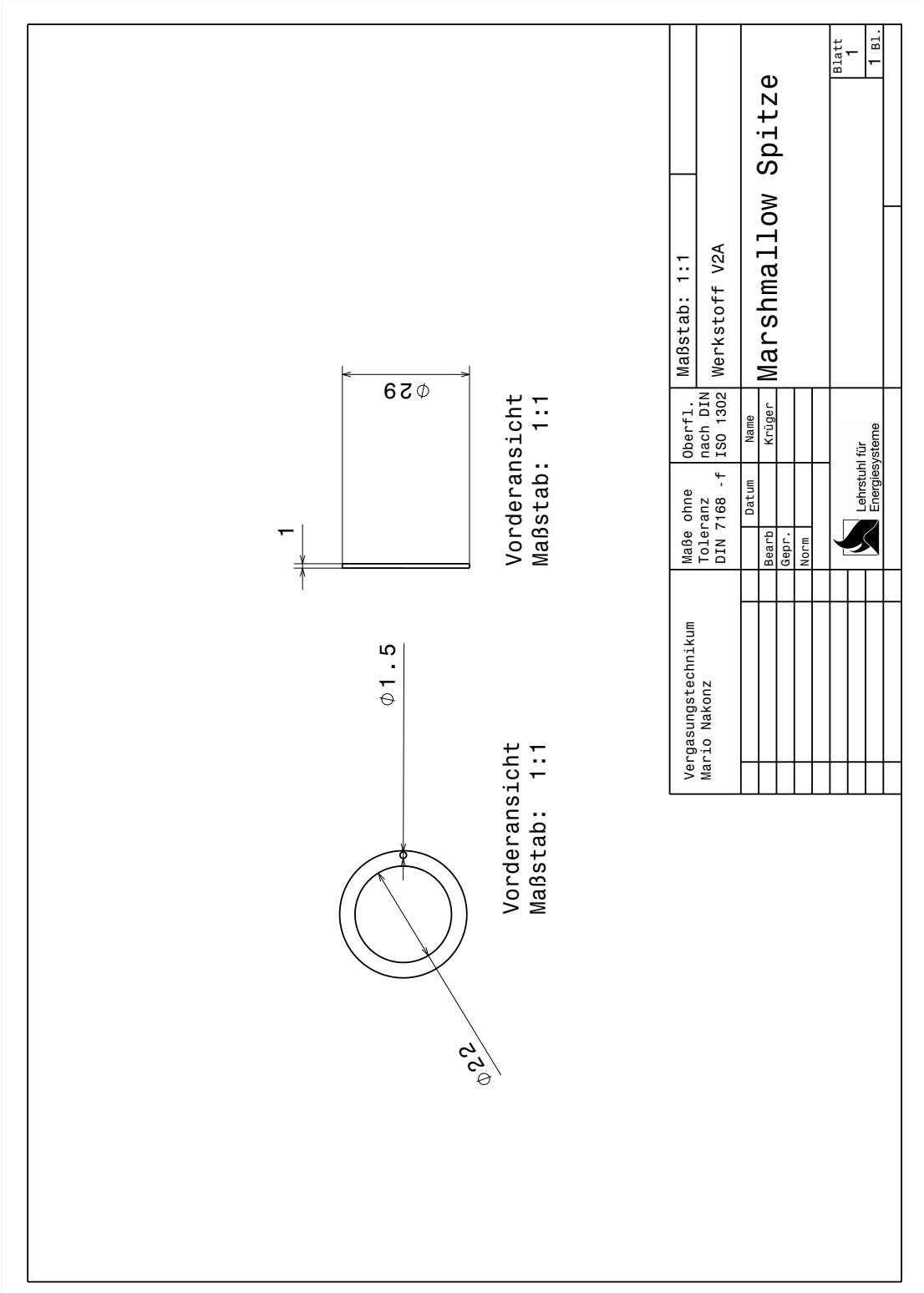

Figure A.3: Top of the getter cage

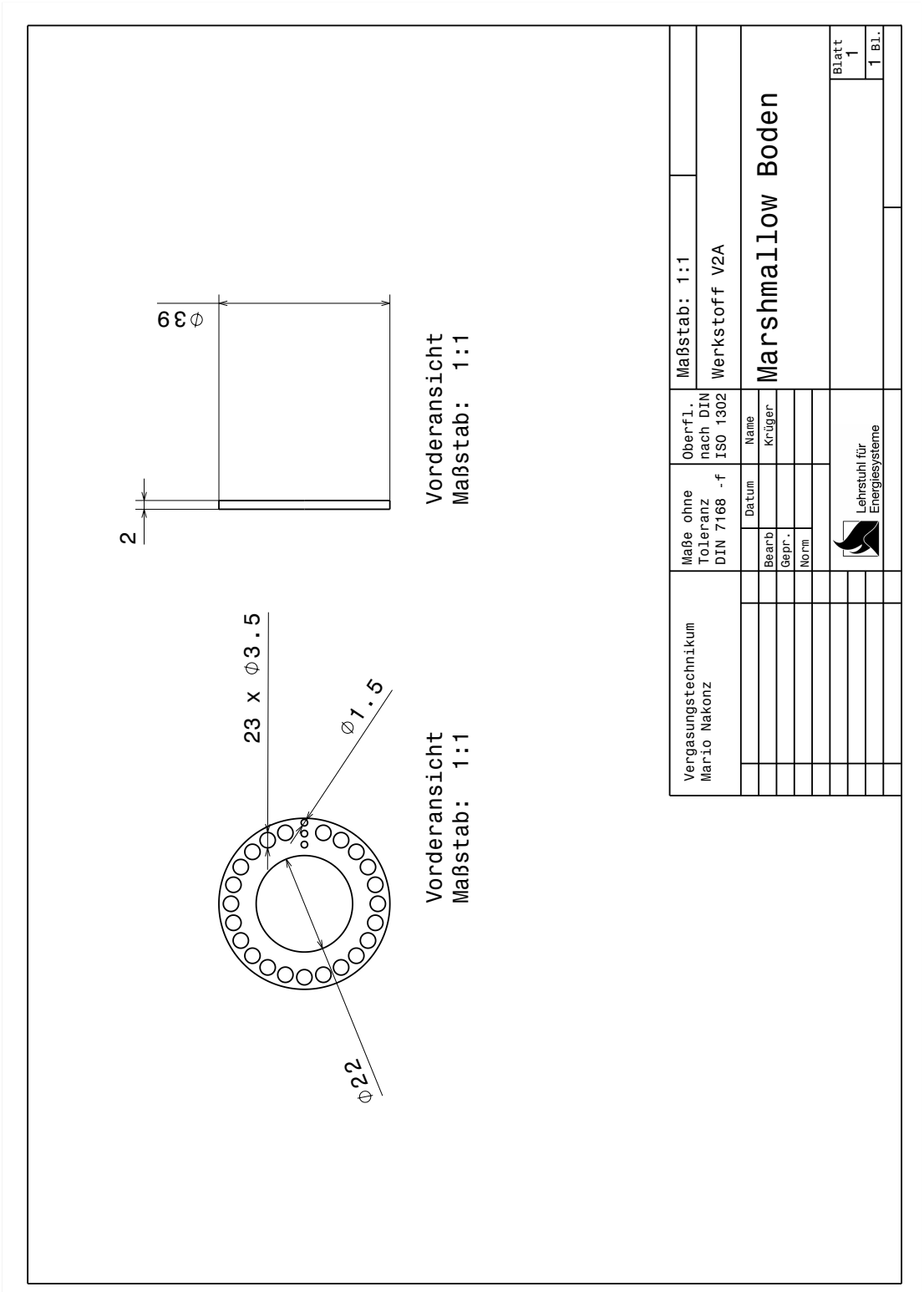

Figure A.4: Bottom of the getter cage

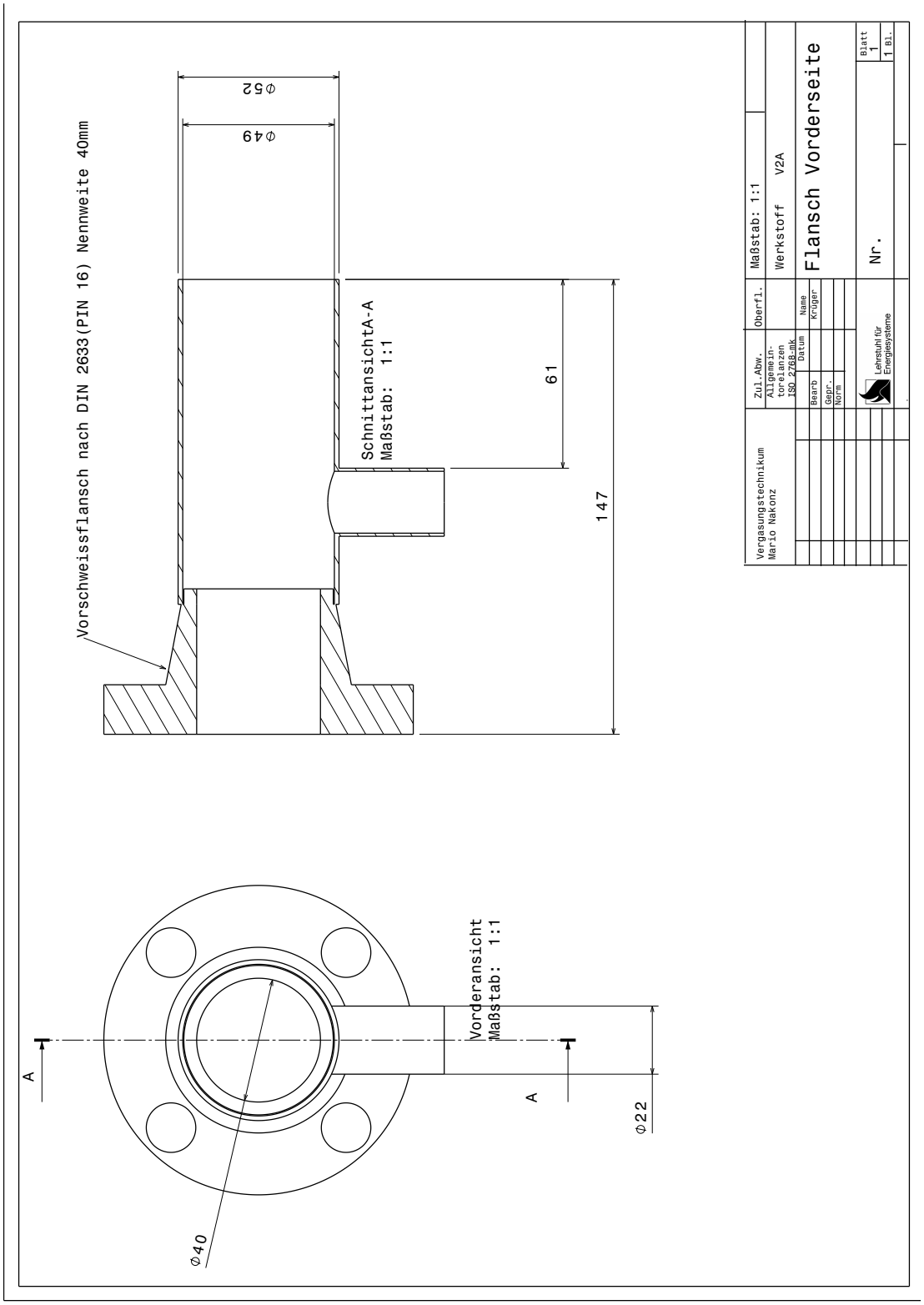

Figure A.5: Front section of measurement system

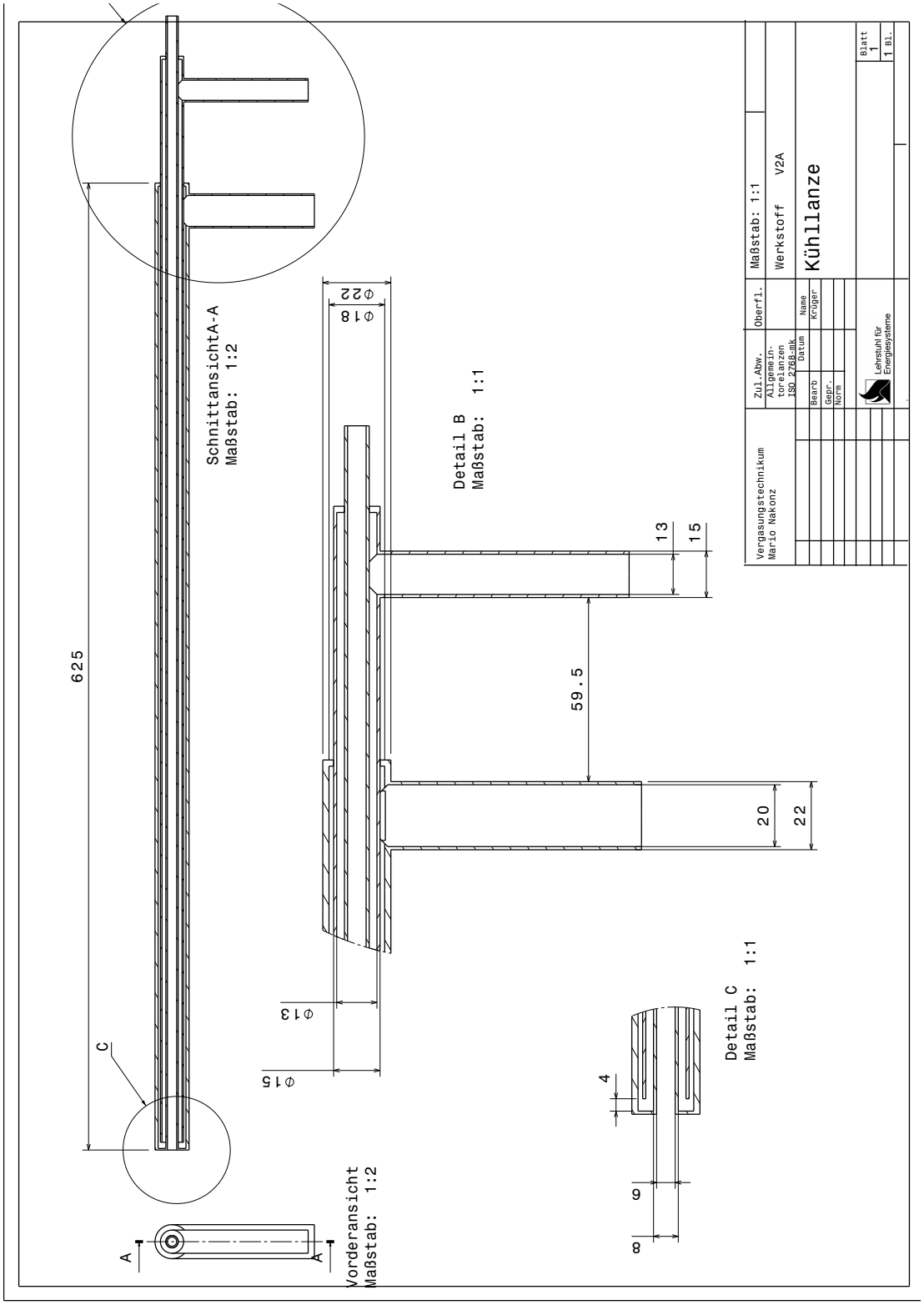

Figure A.6: Cooling probe

A.3 Part Orders

Technische Universität München

Lehrstuhl für Energiesysteme
Fakultät Maschinenwesen

Technische Universität München . Lehrstuhl für Energiesysteme
Boltzmannstraße 15 . 85747 Garching . Germany

ESSKA.de GmbH
Borstelmannsweg 175
20537 Hamburg

Prof. Dr.-Ing.
Hartmut Spliethoff
Tel +49.89.289.16272
Fax +49.89.289.16271
www.es.mw.tum.de

Kundennummer:
133173

Kontaktpersonen:

Cand. Ing. Jonas Krüger
jonaskrueger@mytum.de

Dipl. Ing. Mario Nakonz
Telefon-Durchwahl
+49.89.289.16355
Mario.nakonz@tum.de

Garching, 02.11.2012

Bestellung eines Flanschkugelhahns

Sehr geehrte Damen und Herren,

hiermit bestelle ich folgende Produkte aus ihrem Sortiment:

Bezeichnung	Bestellnummer	Anzahl
Flanschkugelhahn 1-teilig PN 16 DN 40mm	KHFL40_16000	1
Flanschdichtungen DVGW & BAM NW 40mm	FLDR40000009	4

Mit freundlichen Grüßen,

Jonas Krüger

Figure A.7: Order for valve

Technische Universität München

Lehrstuhl für Energiesysteme
Fakultät Maschinenwesen

Technische Universität München . Lehrstuhl für Energiesysteme
Boltzmannstraße 15 . 85747 Garching . Germany

Prof. Dr.-Ing. Hartmut Spliethoff
Tel +49.89.289.16272
Fax +49.89.289.16271
www.es.mw.tum.de

ESSKA.de GmbH
Borstelmannsweg 175
20537 Hamburg

Kundennummer:
133173

Kontaktpersonen:

Dipl. Ing. Mario Nakonz
Telefon-Durchwahl
+49.89.289.16355
Mario.nakonz@tum.de

Cand. Ing. Jonas Krüger
jonaskrueger@mytum.de

Garching, 02.11.2012

Bestellung von Reduzierverschraubungen

Sehr geehrte Damen und Herren,

hiermit bestelle ich folgende Produkte aus ihrem Sortiment:

Bezeichnung	Anzahl	Bestellnummer
Überwurfmutter M10	6	MCK4MSV00000
CK-Schnellverschraubung Schlauch 6mm → G1/4“	6	K144ES000000
Aufschraubverschraubung - Stahl - zöllig (BSP) - L – gerade 8mm → G1/4“	4	858312140808
Aufschraubverschraubung - Stahl - zöllig (BSP) - L – gerade 10mm → G1/4“	1	858312141010
Aufschraubverschraubung - Stahl - zöllig (BSP) - L – gerade 12mm → G1/4“	1	858312141212
Reduzierverschraubung 15mm->8mm	1	858111021508
Reduzierverschraubung 12mm->8mm	1	858111021208
Reduzierverschraubung 10mm->8mm	1	858111021008

Mit freundlichen Grüßen,

Jonas Krüger

Figure A.8: Order for link equipment

Technische Universität München

Lehrstuhl für Energiesysteme
Fakultät Maschinenwesen

Technische Universität München . Lehrstuhl für Energiesysteme
Boltzmannstraße 15 . 85747 Garching . Germany

Prof. Dr.-Ing. Hartmut Spliethoff
Tel +49.89.289.16272
Fax +49.89.289.16271
www.es.mw.tum.de

Fiboflansch-Rohr
Handels GmbH
Königsberger Str. 2
85386 Eching

Kontaktperson:
Dipl. Ing. Mario Nakonz
Telefon-Durchwahl
+49.89.289.16355
Mario.nakonz@tum.de

Garching, 02.11.2012

Bestellung von 2 Vorschweissflanschen

Sehr geehrte Damen und Herren,

hiermit bestelle ich ausgehend von ihrem Angebot vom 08.10.2012 2 Vorschweißflansche nach DIN 2633(PIN16) mit Nennweite 40mm aus 1.4541 V2A.

Mit freundlichen Grüßen

Jonas Krüger

Figure A.9: Order for connections

Technische Universität München

Lehrstuhl für Energiesysteme
Fakultät Maschinenwesen

Technische Universität München . Lehrstuhl für Energiesysteme
Boltzmannstraße 15 . 85747 Garching . Germany

Prof. Dr.-Ing. Hartmut Spliethoff
Tel +49.89.289.16272
Fax +49.89.289.16271
www.es.mw.tum.de

FRIATEC Aktiengesellschaft
Division Keramik
Steinzeugstraße 50
68229 Mannheim

Kontaktpersonen:
Cand. Ing. Jonas Krüger
jonaskrueger@mytum.de

Dipl. Ing. Mario Nakonz
Telefon-Durchwahl
+49.89.289.16355
Mario.nakonz@tum.de

Garching, 02.11.2012

Bestellung von Hochtemperaturkeramikbauteilen

Sehr geehrte Damen und Herren,

hiermit bestelle ich folgende Hochtemperaturkeramikbauteile aus ihrem Lieferprogramm für Standardprodukte.

Bezeichnung	Bestellnummer	Anzahl	Bemerkungen
Rohr, offen, AL23	122-11048-0	1	Länge 200mm
Platte, rund, AL23	211-11045-0600	1	
Isolierperlen, AL23	161-11040-00004	18	
Schiffchen, AL23	221-11050-0150	1	

Mit freundlichen Grüßen

Jonas Krüger

Figure A.10: Order for ceramic material for the probe system tip

Technische Universität München

Lehrstuhl für Energiesysteme
Fakultät Maschinenwesen

Technische Universität München . Lehrstuhl für Energiesysteme
Boltzmannstraße 15 . 85747 Garching . Germany

Prof. Dr.-Ing.
Hartmut Spliethoff
Tel +49.89.289.16272
Fax +49.89.289.16271
www.es.mw.tum.de

ULFALUX Lackfabrik GmbH
Gewerbestr. 6
91452 Wilhermsdorf

Kontaktperson:
Dipl. Ing. Mario Nakonz
Telefon-Durchwahl
+49.89.289.16355
Mario.nakonz@tum.de

Jonas Krüger

Garching, den 29.11.2012

Bestellung von Hochtemperaturfüllspachtel

Sehr geehrte Damen und Herren,

hiermit bestelle ich ausgehend von ihrem Angebot vom 28.11 folgendes Produkt aus ihrem Lieferprogramm.

Bezeichnung	Anzahl
ULFALUX-Füllspachtel 375, feuerfest ca. 1800°C, gebrauchsfertig, 0,4kg Dose	2

Mit freundlichen Grüßen

Jonas Krüger

Figure A.11: Order for high temperature stopper

Technische Universität München

Lehrstuhl für Energiesysteme
Fakultät Maschinenwesen

Technische Universität München . Lehrstuhl für Energiesysteme
Boltzmannstraße 15 . 85747 Garching . Germany

Prof. Dr.-Ing.
Hartmut Spliethoff
Tel +49.89.289.16272
Fax +49.89.289.16271
www.es.mw.tum.de

Profimess GmbH
Twischlehe 5
27580 Bremerhaven

Kontaktpersonen:

Dipl. Ing. Mario Nakonz
Telefon-Durchwahl
+49.89.289.16355
Mario.nakonz@tum.de

Cand. Ing. Jonas Krüger
jonaskrueger@mytum.de

Garching, 29.11.2012

Bestellung von Visi-Float Flowmetern

Sehr geehrte Damen und Herren,

ausgehend von ihrem Angebot vom 28.11.2012 bestelle ich folgende Produkte aus ihrem Sortiment:

Bezeichnung	Anzahl
Visi-Float® Flowmeter Typ: VFB-65-BV Messbereich: 0,2...4 l/min Luft	2

Bitte die Lieferung an

Dipl. Ing. Mario Nakonz
Lehrstuhl für Energiesysteme
Boltzmannstraße 15
85747 Garching

adressieren.

Mit freundlichen Grüßen,

Jonas Krüger

Figure A.12: Order for flow meters, range 0-4 $^{l}/_{\min}$

Technische Universität München

Lehrstuhl für Energiesysteme
Fakultät Maschinenwesen

Technische Universität München . Lehrstuhl für Energiesysteme
Boltzmannstraße 15 . 85747 Garching . Germany

Prof. Dr.-Ing.
Hartmut Spliethoff
Tel +49.89.289.16272
Fax +49.89.289.16271
www.es.mw.tum.de

TC Direct
Postfach 400141
41181 Mönchengladbach

Kundennummer:
18918

Kontaktpersonen:

Cand. Ing. Jonas Krüger
jnskrueger@gmail.com

Dipl. Ing. Mario Nakonz
Telefon-Durchwahl
+49.89.289.16355
Mario.nakonz@tum.de

Garching, 12.10.2012

Bestellung von Temperatursensoren und zugehörigem Equipment

Sehr geehrter Herr Cetinkilic,

hiermit bestelle ich folgende Produkte aus ihrem Sortiment:

Bezeichnung	Bestellnummer	Anzahl
Typ K, Inconel 600 Mantel Länge 1000mm, 1,5mm Durchmesser	405-574	4
Ausgleichsleitung Typ KCB 25m	818-184	1
Vier-Kanal Datenlogger mit Anzeige	4KDATLOG	1
Typ K Standard Kupplung	724-212	4

Mit freundlichen Grüßen

Jonas Krüger

Figure A.13: Order for temperature sensors, type K

A.4 Verification Experiments

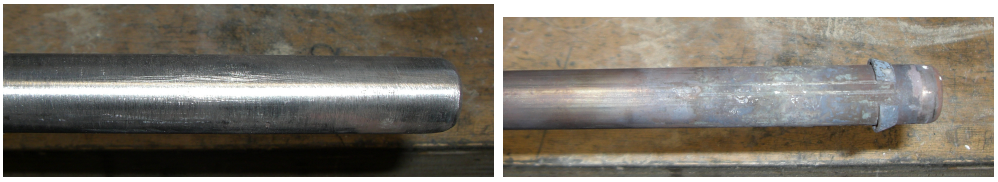

(a) (b)

Figure A.14: Probe tip in different stages of the experiment: (a) Polished probe tip before experiment, (b) Probe tip after 30 minutes at 1400 °C and NaCl

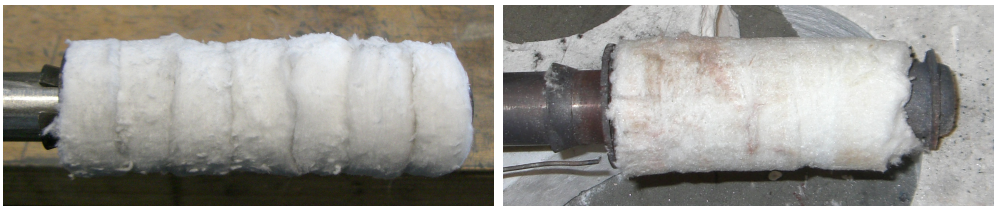

(a) (b)

Figure A.15: Marshmallow tip in before and after experiments with sodium chloride: (a) Marshmallow principle before experiment, (b) Marshmallow principle after 30 minutes at 1400 °C and NaCl

Figure A.16: Samples of the getter material after experiment at 1400 °C and 30 minutes exposure to NaCl

A.5 Source code of the UDFs

A.5.1 Volume_UDF

```
#include "udf.h"
//DEFINE REACTION RATE ON THE SURFACE for ALL THE REACTION
DEFINE_VR_RATE(cond_antoine,c,t,r,my,yk,rr,rr_t)
{
real psatNaCl,psatKCl,p_operating,ptot,pi;
real T;
real massKCl;
real massNaCl;
real save_rr_NaCl,save_rr_NaCl_t,save_rr_KCl,save_rr_KCl_t;

/* A,B,C Antoines Coefficients for NaCl at T>800 C */
//http://webbook.nist.gov/cgi/cbook.cgi?ID=C7647145&Mask=4#Thermo
   -Phase

real ANaCl=3.56682;
real BNaCl=5200.9;
real CNaCl=-317.409;

/* A,B,C Antoines Coefficients for KCl at T>800 C */

real AKCl=4.78236;
real BKCl=7440.691;
real CKCl=-122.709;
real xsatNaCl;
real xsatKCl;
real d;
//C_UDMI(c,t,0) = 0.0;
//C_UDMI(c,t,1) = 0.1;
//C_UDMI(c,t,2) = 0.2;
//C_UDMI(c,t,3) = 0.3;
//C_UDMI(c,t,4) = 0.4;
//C_UDMI(c,t,5) = 0.5;
T=C_T(c,t);

if (T<400)
```

```
{
T=400;
}

/* Antoines Law: Log(P)= A-(B/(C+T)) */
psatNaCl=(pow(10,(ANaCl-(BNaCl/(T +CNaCl)))))*100000;

//Message("pressure");
p_operating = RP_Get_Real("operating-pressure");
ptot= C_P(c,t)+p_operating;

xsatNaCl=psatNaCl/ptot;
C_UDMI(c,t,0) = xsatNaCl;

d=sqrt(C_Volume(c,t));
//Message("rr");
*rr=0.0;
*rr_t=0.0;
//Message("udmi");
//NaCl-->NaCl<s>

//excess compound in gas phase
massNaCl = yk[0]-(xsatNaCl*(my[0]/my[2]));
C_UDMI(c,t,1) = massNaCl;

//Calculation of reaction rate, only qualitative!
save_rr_NaCl = 0.01 * (C_R(c,t) * C_DIFF_EFF(c,t,0) * massNaCl /
   d) / my[0];
save_rr_NaCl_t = 0.01 * (C_R(c,t) * C_DIFF_EFF(c,t,0) * massNaCl
   / d) / my

[0];
C_UDMI(c,t,2)=save_rr_NaCl;

if(massNaCl >= 0)
{
*rr = save_rr_NaCl;
*rr_t = save_rr_NaCl_t;
}
```

```
if      (THREAD_VAR(t).fluid.porous)
{
        *rr = 0.0;
        *rr_t = 0.0;
}
}

/*-------------------------------------------------------------------*/
/* for KCl-calculations comment the code above and uncomment the
   code

below*/
/* Antoines Law: Log(P)= A-(B/(C+T)) */
/*
psatKCl=(pow(10,(AKCl-(BKCl/(T +CKCl))))*100000;

//Message("pressure");
p_operating = RP_Get_Real("operating-pressure");
ptot= C_P(c,t)+p_operating;

xsatKCl=psatKCl/ptot;
C_UDMI(c,t,0) = xsatKCl;

d=sqrt(C_Volume(c,t));
//Message("rr");
*rr=0.0;
*rr_t=0.0;
//Message("udmi");
//KCl-->KCl<s>

//excess compound in gas phase
massKCl = yk[0]-(xsatKCl*(my[0]/my[2]));
C_UDMI(c,t,1) = massKCl;

//Calculation of reaction rate, only qualitative!
save_rr_KCl = 0.01 * (C_R(c,t) * C_DIFF_EFF(c,t,0) * massKCl / d)
    / my[0];
save_rr_KCl_t = 0.01 * (C_R(c,t) * C_DIFF_EFF(c,t,0) * massKCl /
   d) / my[0];
```

```
C_UDMI(c,t,2)=save_rr_KCl;

if(massKCl >= 0)
{
*rr = save_rr_KCl;
*rr_t = save_rr_KCl_t;
}
if      (THREAD_VAR(t).fluid.porous)
{
        *rr = 0.0;
        *rr_t = 0.0;
}
}*/
```

A.5.2 Surface_condensation_UDF

```
/*
   ************************************************************

  Custom surface reaction rate UDF

   ************************************************************
   */
#include "udf.h"
DEFINE_SR_RATE(porous_cond,c,t,r,my,yi,rr)
{
        *rr = 0.0;

if      (FLUID_THREAD_P(t)      &&      THREAD_VAR(t).fluid.
   porous)
        {
        *rr     = - C_UDMI(c,t,2);
        }
}}
```